This is a postprint. The article was submitted for peer-review to the *Journal of Luminescence* and is now published as:

Riedesel, S., Duller, G.A.T., Ankjærgaard, C., 2023. *Time-resolved infrared stimulated luminescence of the blue and yellow-green emissions – insights into charge recombination in chemically and structurally different alkali feldspars.* Journal of Luminescence 257, 119724.

The article can be accessed by using its DOI: https://doi.org/10.1016/j.jlumin.2023.119724

Time-resolved infrared stimulated luminescence of the blue and yellow-green emissions – insights into charge recombination in chemically and structurally different alkali feldspars

Svenja Riedesel[1,2], Geoff A.T. Duller[2], Christina Ankjærgaard[3]

[1] Institute of Geography, University of Cologne, Albertus-Magnus-Platz, 50923 Köln/Cologne, Germany

[2] Department of Geography and Earth Sciences, Aberystwyth University, Penglais Campus, Aberystwyth SY23 3DB, United Kingdom

[3] Department of Health Technology, Technical University of Denmark, Risø Campus, 4000 Roskilde, Denmark

Corresponding author: Svenja Riedesel, riedeselsvenja@gmail.com

Abstract

Time-resolved luminescence measurements can be used to explore luminescence processes in minerals and the defects involved. It has also been applied to feldspars and knowledge has been gained regarding potential crystal defects associated with luminescence productions in these minerals, but also regarding processes governing electron-hole recombination leading to luminescence emission.

Here we present time-resolved infrared stimulated luminescence (IRSL) signals measured for a range of mineralogically well characterised single crystal alkali feldspars. We explore time-resolved luminescence for the blue (~410 nm) and the yellow-green emission (~550 nm) in response to different irradiation doses and by comparing different IRSL signals. Firstly, we explore whether the lifetimes measured represent excited state or recombination lifetimes. Secondly, we investigate sample-dependent changes in blue and yellow-green time-resolved signals and link those to physical properties of the samples.

Our results show that the timescales on which the blue and the yellow-green emission occur differ significantly, with the blue signal on the µs-scale, and the yellow-green emission on the ms-scale. We

do not observe any dependence of the time-resolved signal on signal integration, dose given or IRSL signal measured. However, inter-sample variability is shown for both emissions. In the blue we only observe small differences in decay time scale between single-phase feldspars and perthites, however larger differences are measured between samples that were artificially disordered compared to ordered feldspars. Longer lifetimes observed for disordered feldspars are suggested to be linked to either changes in the recombination centre or to increased band-tail states transport due to an increase in the width or density of the sub-conduction band-tail states. The data indicates the potential of using time-resolved IRSL of the blue emission to get an indication of the state of order of a feldspar. For the yellow-green emission slow signal decays are observed for single-phase feldspars, likely indicating a spin-forbidden transition. Interestingly, similar lifetimes were observed for K- and Na-feldspar end members.

Keywords

Time-resolved luminescence, lifetime, feldspar, recombination, band-tail states

1 Introduction

Conventional optically stimulated luminescence measurements use continuous wave (CW) stimulation to excite trapped electrons and enable their migration through the crystal lattice, resulting in recombination at a recombination centre. If the recombination process is radiant it leads to the emission of photons. In time-resolved luminescence measurements samples are stimulated using pulsed light, meaning that a time-resolved measurement consists of multiple stimulation light pulses, separated by so-called off-times, during which no optical stimulation occurs (Sanderson and Clark, 1994; Lapp et al., 2009). This method not only enables an improved discrimination of excitation and emission wavelengths, but also gives information on recombination processes in minerals (Sanderson and Clark, 1994). During on-times of pulsed stimulation, electrons are excited from the ground state of the electron trapping centres and migrate to recombination centres, while the off-time allows investigations into the decay of different luminescence emissions after the optical stimulation has been turned off. Thus, time-resolved luminescence measurements make it possible to measure recombination lifetimes and excited state lifetimes of the luminescence centres.

Feldspars are the most abundant mineral in the Earth's crust. Feldspars are complex framework silicates, which occur in a variety of forms along two solid solution series ($KAlSi_3O_8$ – $NaAlSi_3O_8$, termed alkali feldspars, and $NaAlSi_3O_8$ – $CaAl_2Si_2O_8$, termed plagioclase). The chemical composition and water content of the melt, pressure conditions and temperature gradients during cooling influence the type of feldspar which crystallises from the melt (e.g. Deer et al., 2013). The temperature gradient at which feldspars cool dictate their structural state: the site occupancy of Al^{3+} ions on the (Si, Al)-framework.

Feldspars with a high structural state have a disordered framework, whereas feldspars with a low structural state are ordered (cf. high sanidine compared to low microcline, high albite compared to low albite). To accommodate K^+ and Na^+ ions, which have very different ionic radii, in the alkali feldspar crystal during cooling, exsolution occurs and perthites form (e.g. Deer et al., 2013). Especially alkali feldspars have been studied extensively for geochronological applications (e.g. Godfrey-Smith et al., 1988; Hütt et al., 1988; Duller, 1997; Buylaert et al., 2012). For feldspars, time-resolved luminescence measurements have previously been performed to gain insights into electron-hole recombination processes (e.g. Sanderson and Clark, 1994; Jain and Ankjærgaard, 2011) and to understand defects involved in luminescence production and their locations within the crystal lattice (e.g. Clark and Bailiff, 1998). Despite this previous research, it is still unknown, how different chemistry and structure of feldspars impact luminescence production and how these factors influence excited state and recombination lifetimes of feldspar infrared stimulated luminescence (IRSL). In this paper we use time-resolved IRSL with detection in the blue (~410 nm) and yellow-green (~550 nm) wavelength regions to explore recombination processes and potentially involved defects in chemically and structurally different alkali feldspars.

Time-resolved luminescence of feldspars with emissions in the UV, blue, yellow-green or red to near-infrared, have been investigated, mainly to understand the defects and transitions involved in the recombination process (cf. Clark et al., 1997; Clark and Bailiff, 1998; Tsukamoto et al., 2006; Prasad et al., 2016). The blue luminescence emission has been associated with a hole centre located on Al-O-Al bridges (Finch and Klein, 1999; Riedesel et al., 2021a) and it has been shown that its intensity and stability is dependent on the degree of order on the Si, Al-framework and on the presence and type of interfaces in perthites (Riedesel et al., 2021a). However, it is unknown whether lifetimes of the blue emission are also affected by changes to the crystal structure. Previous research investigating lifetimes of the blue emission indicated very fast decaying signals with lifetimes on the sub-µs to few µs-scale (e.g. Clark et al., 1997; Clark and Bailiff, 1998). Besides those very fast lifetimes, Ankjærgaard and Jain (2010) observed very long lifetimes for the blue emission on the ms- to s-scale. These authors suggest band-tail state transport as the source of these long lifetimes.

For the yellow-green emission two likely defect sites have been proposed: (i) The emission at ~560 nm has been assigned to Mn^{2+} substituting for Ca^{2+} in plagioclases resulting in a spin-forbidden transition with long lifetimes on the ms-scale (e.g. Geake et al., 1971, 1973, 1977; Telfer and Walker, 1978). These long lifetimes are due to the transition within the 3d shell, linked to the electrons being influenced by the crystal field strength, site symmetry and them being strongly coupled to lattice vibrations (Shi et al., 2010) ; (ii) Alternatively, the emission was suggested to result from Mn^{2+} substituting for Al^{3+} on tetrahedral sites (T sites) in alkali feldspars, creating a lattice stabilising hole centre on Si^{4+}-O^--Mn^{2+}

(Telfer and Walker, 1978; Kirsh et al., 1987). This second possibility would result in shorter lifetimes, due to the defect being located at a lattice site. Clark and Bailiff (1998) have indeed observed very fast lifetimes (on the ns-scale) for the emission at ~560 nm, supporting a lattice site defect for the yellow-green emission. From phosphorescence data Prasad et al. (2016) observed dominant lifetimes of the yellow-green emission of the order of hundreds of microseconds to less than a fraction of a millisecond – also an observation against a spin forbidden transition of a defect located on cation sites (M sites). Riedesel et al. (2021a) observed a strong yellow-green emission centred around 560 nm in alkali feldspar end members albite and microcline, with all three samples having zero to negligible concentrations of MnO as determined by X-ray fluorescence analysis. Thus, the source of the yellow-green emission in chemically different alkali feldspars needs further investigation.

Besides using time-resolved luminescence to link certain defect types to luminescence emissions, feldspar time-resolved luminescence has been used to improve the understanding of electron-hole recombination processes and to infer possibilities to extract a more stable luminescence signal for dating. As part of this work, it has been debated whether the time-resolved luminescence signal of feldspars represents the excited state lifetime of the luminescence centre (the time needed for the electron to transition from the excited state to the ground state of the luminescence centre, cf. e.g. Clark et al., 1997) or the recombination lifetime (the time needed for the excited electron to move from the electron trapping centre to a recombination centre) (e.g. Ankjærgaard et al., 2009; Tsukamoto et al., 2010), and which role band-tail states play in this process (e.g. Jain and Ankjærgaard, 2011; Pagonis et al., 2012).

The current understanding of feldspar luminescence is primarily based on a proximity model, where the electron-hole pairs are separated by a distribution of distances and where it is understood that recombination will occur at the nearest recombination centre (e.g. Huntley, 2006; Jain et al., 2012). Feldspars containing a higher density of recombination centres will thus have less stable luminescence signals, compared to feldspars with a lower density, because it will be more likely for electrons to recombine at a proximal luminescence centre, even more likely through tunnelling processes (e.g. Huntley, 2006; Jain et al., 2012). Subsequently, one would expect faster recombination lifetimes in a system with a higher density of recombination centres, compared to systems with a lower recombination centre density. Ankjærgaard et al. (2009) explored whether the time-resolved luminescence signal of feldspars (green (532 nm) laser or blue (470 nm) LED stimulation and UV detection) reflected the excited state or the recombination lifetime. They found arguments for either of the two processes controlling the lifetimes measured. One argument supporting the recombination lifetime hypothesis was shown by time-resolved optically stimulated luminescence (OSL) measured at different stimulation temperatures resulting in the same decay shape, i.e. not giving rise to thermal

quenching. However, Ankjærgaard et al. (2009) also found counter arguments, thus supporting the excited state lifetime hypothesis: A systematic decrease in lifetime with increasing preheat temperature was observed for feldspar time-resolved OSL. The authors argued that longer lifetimes were expected for higher preheat temperatures, as a high preheat would result in a depletion of recombination centres, making recombination more difficult and thus increasing the recombination lifetime. Ankjærgaard et al. (2009) further explored whether different stimulation times could affect the lifetimes and decay shape of the signals, expecting an increase in lifetimes with increasing stimulation time. If the lifetimes measured would correspond to recombination lifetimes, then one would expect longer lifetimes with decreasing hole concentrations due to longer stimulation lifetimes. However, no clear trend was observed. Tsukamoto et al. (2010) compared time-resolved OSL and time-resolved OSE (optically stimulated exo-electron) measurements of quartz, feldspar and NaCl and found that the decay of time-resolved OSE signals are faster than time-resolved OSL in the case of NaCl and quartz, with time-resolved OSE signals decaying on timescales <1 μs, while NaCl and quartz time-resolved OSL signals decay with a lifetime of ~40 μs. time-resolved OSE and time-resolved OSL of feldspars decay on similar timescales. The very fast decaying time-resolved OSE signals are understood as rapid emptying of the electron population in the conduction band immediately after turning off the stimulation light source. In contrast, the slower decay of the time-resolved OSL signals is interpreted as arising from relaxation processes within the recombination centre, thus being governed by the excited state lifetime of these defects and the internal transitions.

Since the physical source of various time-resolved luminescence signals is still under debate, and it is still unclear whether the off-time of time-resolved signals represents the excited or the recombination lifetime, different approaches have been used to describe time-resolved luminescence signals, particularly focussed on the off-time signal. Most commonly a sum of multiple first order exponential functions have been used to describe the time-resolved off-time signal (e.g. Clark et al., 1997; Clark and Bailiff, 1998; Tsukamoto et al., 2006; Ankjærgaard et al., 2009). However, feldspar luminescence is not a first order process (e.g. Huntley, 2006) and thus it has been proposed that fitting a sum of multiple first order exponential functions might be inappropriate (e.g. Ankjærgaard, 2009; Pagonis et al., 2012, 2016). Jain and Ankjærgaard (2011) thus visually separated the off-time signal into a “fast” and a “slow” time-resolved signal, with the “fast” signal describing the initial decay, and the “slow” signal governing the time-resolved signal after 70 μs in the off-time. Pagonis et al. (2012) applied a linear combination of exponential and stretched exponential functions. These authors interpreted the part of the time-resolved signal fitted by a stretched exponential as being caused by transport via the band-tail states. Later Pagonis et al. (2016) developed analytical equations describing feldspar time-resolved luminescence, which are based on the nearest-neighbour recombination model by Jain et al. (2012). However, there are still many unknowns in the physical processes involved in luminescence

production in feldspars, so no definite answer can yet be given regarding the optimal signal analysis procedure.

The research presented in this paper is focussed on creating a better understanding of defects and processes involved in blue and yellow-green luminescence production. Therefore, we measure time-resolved luminescence resulting from pulsed IR stimulation with emissions in the blue and yellow-green wavelength region of a suite of representative single crystal alkali feldspars including single-phase feldspars, perthites and artificially disordered feldspars. These are explored to investigate whether the measured time-resolved luminescence signal and its lifetimes and decay shape are governed by the recombination or excited state lifetime and which role band-tail states might potentially play. We compare time-resolved luminescence resulting from different IRSL signals, different irradiation doses and of chemically and structurally different feldspars.

2 Materials and methods

2.1 Samples

Samples investigated here are single crystal alkali feldspar specimens. Their chemical composition, structural state and mineral phases present have been characterised previously and details can be found in Riedesel et al. (2021a). The sample suite represents the chemical and structural range of the alkali feldspar solid solution series and its end members. The chemical composition, mineral phases present and the structural state of the samples was determined using X-ray fluorescence and X-ray diffraction and a summary of the results is given in Table 1. FSM-13 is a single-phase microcline (98.5 % K-feldspar) and CLBR a single-phase albite (0.5 % K-feldspar). FSM-3 (82.5 % K-FS), FSM-6 (74.4 % K-FS) and FSM-5 (74.8 % K-FS) are perthites. FSM-3 and FSM-6 are cryptoperthites consisting of albite and microcline (FSM-3) or orthoclase (FSM-6). FSM-5 is a macroperthite consisting of albite and microcline. FSM-13LH and FSM-6LH are artificially disordered samples. To obtain these samples, powdered sample material of FSM-13 and FSM-6 was heated in Pt crucibles in a furnace to 1050 °C and then rapidly cooled to room temperature to retain the disordered high-temperature structure, with Al^{3+} ions distributed randomly across tetrahedral sites on the (Si,Al)-framework. Details of these experiments and a comparison of the X-ray diffraction pattern of the ordered/disordered sample pairs can be found in Riedesel et al. (2021a). For each sample three aliquots were measured.

Table 1. Details regarding the chemical composition and mineral phases present for samples investigated. The chemical composition in % feldspars, was done using stoichiometric conversion of the semi-quantitative XRF data. Present phases estimated based on semi-quantitative XRD analyses.

Sample ID	Origin	Chemical composition (FS %)			Phases present			
		K-FS	Na-FS	Ca-FS	Microcline	Orthoclase	Sanidine	Albite
FSM-13	Brazil	98.5	1.5	0.0	100.0	-	-	
FSM-13LH	Brazil	98.5	1.5	0.0	100.0	-	-	

FSM-3	Granite pegmatite, Toe Head, South Harris, Scotland, UK (Cunningham, 1981)	82.5	17.2	0.3	78.0	-	-	22.0
FSM-5	Unknown	74.8	25.20	0.0	57.0	-	-	43.0
FSM-6	Granite pegmatite, Trezaise Quarry, Cornwall, UK (see Ussher et al., 1909)	74.4	25.3	0.3	-	38.0	-	62.0
FSM-6LH	Trezaise Quarry, Cornwall, UK	74.4	25.3	0.3	-	-	100.0	-
CLBR	Pegmatite, Golonca District, Minas Gerais, Brazil (Cassadanne and Roditi, 1996)	0.5	99.3	0.2	-	-	-	100

199

200 **2.2 Instrumentation and measurement protocol**

201 Time-resolved luminescence measurements were made on a Risø TL/OSL DA20 reader equipped with
202 a $^{90}Sr/^{90}Y$ beta source delivering ~0.1 Gy s^{-1} at the sample position and a Detection And Stimulation
203 Head (DASH) including an automated filter changer (Lapp et al. 2015). For the measurements
204 presented in this paper infrared stimulated luminescence (IRSL) was detected using a PDM 9107Q-AP-
205 TTL-03 (sensitive wavelength region: 160-630 nm) photomultiplier tube. For detection of the blue
206 emission (~410 nm) we used a combination of Schott BG39 (2 mm) and BG3 (3 mm) filters and for the
207 yellow-green emission (~550 nm) a combination of Schott BG39 (2 mm) and OG550 (2 mm) filters.
208 Dependent on the brightness of the sample ND 1.0 or ND 2.0 filters were added to the chosen filter
209 combination. The emission windows of the individual filters and the chosen filter combinations are
210 displayed in Figs. 1D and 1E and a comparison of the transmission on linear and logarithmic scales can
211 be found in Fig. S1 in the supplementary material. The stimulation was achieved using 850 nm (300
212 mW cm^{-2}) IR LEDs, operating at 90 % power.

213 Time-resolved luminescence measurements were possible through a photon timer attachment
214 (TimeHarp 260) in combination with the pulsed optically stimulated luminescence (OSL) unit (Lapp et
215 al., 2009). The TimeHarp 260 photon timer enables the detection of individual photons with a time
216 resolution of up to 1 ns. The pulsed IRSL plug-in board allows on- and off-times to be adjusted between
217 0.6 µs and 10 s. Additionally, different gating intervals can be selected. For time-resolved IRSL
218 measurements with emission detection in the blue wavelength region we used on-times of 50 µs,
219 followed by an off-time of 200 µs. Due to the much slower decay of the yellow-green time-resolved
220 IRSL signal, on-times were 5 ms, followed by an off-time of 45 ms. By defining these on-times for the
221 blue and yellow-green emissions, respectively, we ensured that the time-resolved signal in some of
222 the samples investigated reached a stable on-time signal, prior to switching off the LEDs. The time-
223 resolved IRSL signals for both emissions were recorded over a total stimulation time of 200 s.

Time-resolved IRSL measurements were performed using a post-$IR_{50}IRSL_{225}$ protocol with a 60 s preheat at 250 °C. The IR stimulation time was 200 s for the $IRSL_{50}$ and post-IR $IRSL_{225}$ signals. Prior to each measurement using the post-IR IRSL protocol the samples were annealed to 450 °C to ensure complete signal resetting (Table 2). All samples were irradiated after the 450 °C clean-out. Blue time-resolved IRSL measurements were performed after irradiation doses of 50, 200 and 800 Gy. Yellow-green time-resolved IRSL measurements were conducted after doses of 200 or 800 Gy. In case of samples FSM-5 and FSM-6 the yellow-green emission was not intense enough after a dose of 200 Gy, thus these samples were irradiated with 400 Gy instead. Results of these dose-dependent measurements are presented in section 3.1.3 for the blue emission. Results of these experiments for the yellow-green emission are not shown, but results obtained from fitting are given in Tables S3a and S3b in the supplementary material.

Table 2: Measurement protocol used.

Step	Treatment	Purpose
1	TL to 450 °C, 1 °C s^{-1}	Signal clean out
2	Beta dose 50, 200, 400 or 800 Gy	Irradiation, dose dependent on experiment
3	Preheat to 250 °C, 2 °C s^{-1}, 60 s	
4	$IRSL_{50}$, 2 °C s^{-1}, 200s Blue emission: 50 µs on-time, 200 µs off-time Yellow-green emission: 5 ms on-time, 45 ms off-time	Obtain time-resolved $IRSL_{50}$ signal
5	post-IR $IRSL_{225}$, 2 °C s^{-1}, 200s Blue emission: 50 µs on-time, 200 µs off-time Yellow-green emission: 5 ms on-time, 45 ms off-time	Obtain time-resolved post-IR $IRSL_{225}$ signal

Fitting of time-resolved luminescence signals was done in R using the nls() function (Bates and DeRoy, 2018) using equation 1 for the on-time signal and equation 2 for the off-time signal, where I is the intensity at time t, A_i is the saturation intensity of the i'th component and a_i the intensity at time t_1, where t_1 is the on-time duration, and k is a constant, representing a stable linear background (Chithambo, 2003; Tsukamoto et al., 2006). The data were normalised to the intensity of the last data point of the on-time. The sole purpose of fitting the data was to enable a numerical comparison between the samples used in this paper and to also be able to compare the data obtained here to previously published time-resolved IRSL data (e.g. Clark and Bailiff, 1998; Tsukamoto et al., 2006, 2010). It is not our intention to make any suggestions regarding the physical processes by using the numerical results obtained through fitting the data using a sum of multiple first order exponentials. Later sections discussing potential physical properties of the samples and their influence on the time-

resolved luminescence signals are based on qualitative descriptions and sample-to-sample comparisons.

$$I(t) = \sum A_i \left[1 - \exp\left(\frac{-t}{\tau_1}\right)\right] \quad [1]$$

$$I(t) = \sum a_i \exp\left[-\left(\frac{t-t_1}{\tau_1}\right)\right] + k \quad [2]$$

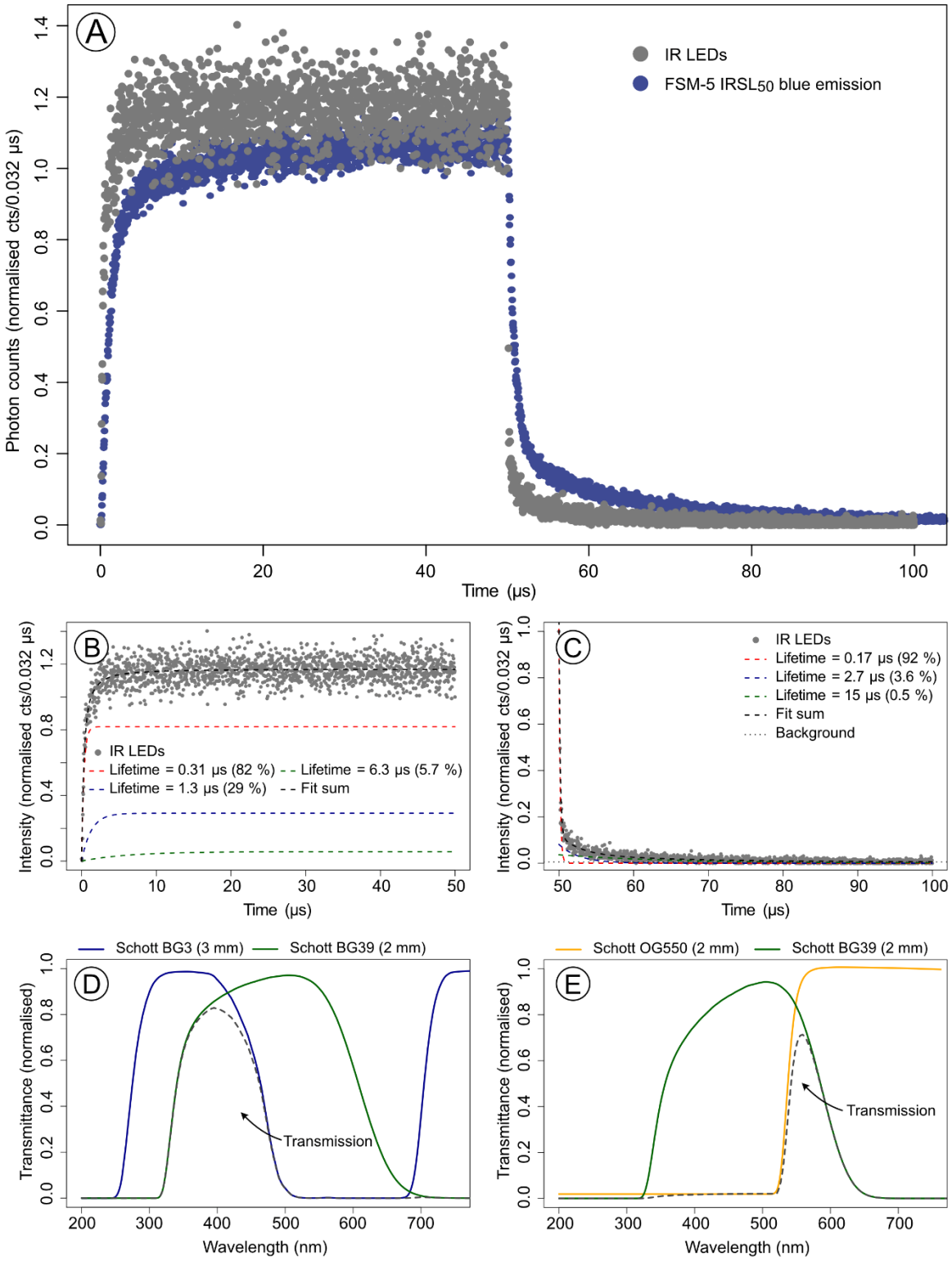

Fig. 1. A) The response of the IR LEDs measured through a ND filter for deadtime correction, and the signal was recorded using a red-sensitive photomultiplier tube (PMT). The signal of FSM-5, the fastest decaying signal from all samples measured, was recorded through the BG39 + BG3 combination visualised in D and was detected using a UV-sensitive PMT. This sample was chosen in comparison as it has the fastest decay in the off-time. B) Fitted LED on-time and C) off-time signal. The signal was normalised to the last point of the on-time, and the scatter of the data means that some measurement points lie above 1. D) Transmission of the BG3 and BG39 filter combination. E) Transmission of the OG550 and BG39 filter combination.

3 Blue time-resolved IRSL emission – Results and Discussion

The blue luminescence emission (~410 nm) is the emission commonly detected when using feldspars for luminescence dating, thus this emission and potential variations of this emission between different feldspars is of particular interest. In the following we investigate variations in the lifetimes of on- and off-times of the blue time-resolved IRSL signals as a function of integration interval, irradiation dose, and IRSL signal investigated. To enable a direct comparison all on- and off-time signals were fitted using a sum of multiple first order exponential functions. We have also attempted to use a linear sum of single exponential function and stretched exponential function (Pagonis et al., 2012) to describe our data. However, fitting our data using the equation given by Pagonis et al. (2012) in R and SigmaPlot yielded parameter values of infinity. The only samples we were able to fit using a linear sum of single exponential function and stretched exponential function were the disordered samples FSM-13LH and FSM-6LH. Thus, we only present lifetimes based on fitting with a linear sum of multiple first order exponential functions.

3.1 Lifetimes

In the following we first investigate the effects of changing the integration interval, the IRSL signal ($IRSL_{50}$ compared to post-IR $IRSL_{225}$) or the given dose on the on- and off-time lifetimes. To enable a numerical comparison, we here use the results obtained from fitting using a sum of multiple exponentials.

All results presented in the following sections are based on time-resolved luminescence signal fitting using between one and four exponential functions (eq. 1 and 2). The number of components used for fitting is based on the lowest residual signal obtained from fitting with different numbers of components, thereby avoiding redundancy in the fitting. Using this approach, we obtained lifetimes ranging from 0.5 µs to over 100 µs. Faster lifetimes could not be detected due to the decay time of the IR LEDs (~0.3 µs, cf. Fig. 1A, B, C). Generally, lifetimes could be arranged into three lifetime groups for the on-time signal: <5 µs, 8-20 µs and > 20 µs, and into four lifetime groups for the off-time: < 1 µs, 3-9 µs, 12-16 µs and > 20 µs. This grouping was done by identifying similar lifetimes between different samples and between the two signals investigated. The grouping is only used for visualisation purposes in figures and tables. Differences in on- and off-time lifetimes might be related to the different time

intervals used for on- and off-times: 50 µs on-time compared to 200 µs off-time, leading to an improved description of the longer off-time duration compared to the shorter on-time. All numerical fitting results can be obtained from the supplementary material.

Integration intervals

The time-resolved IRSL signals were recorded over a stimulation period of 200 s, for the $IRSL_{50}$ and post-IR $IRSL_{225}$ signal, respectively. An example of IRSL decay curves measured during the on- and off-time is given for sample FSM-13 in Fig. S2. Using the software PTanalyse, we extracted photon arrival time distributions of the following time intervals for a comparison: 0-2 s, 0-5 s, 0-10 s, 0-50 s and 0-200 s, 10-50 s, 50-100 s and 100-200 s. To be able to make an absolute comparison, we selected two samples, FSM-3 and CLBR, and fitted the extracted photon arrival time distributions of the on- and off-time of the $IRSL_{50}$ and post-IR $IRSL_{225}$ signals using equation 1 and 2. Figure S3 in the supplementary material shows the results of FSM-3, results for CLBR are not shown, but are similar to those of FSM-3. We did not observe any significant and consistent changes in lifetime with integration interval selected for either of the IRSL signals or any samples. However, increasing the integrated time interval resulted in a better goodness of fit, expressed as the square sum of residuals of the fit, with the best fit obtained when integrating the photon arrival time distribution of the entire IRSL signal (total 200 s stimulation). Subsequently, all data presented in this paper are based on whole IRSL signal integration.

Signals investigated – $IRSL_{50}$ compared to post-IR $IRSL_{225}$

Post-IR IRSL signals are observed to be more stable compared to the $IRSL_{50}$ signal measured as part of the post-IR IRSL protocol (e.g. Thomsen et al. 2008), likely due to the post-IR IRSL signal probing more distant electron-hole-pairs (Jain and Ankjærgaard, 2011). Time-resolved IRSL signal differences have also been observed: Jain and Ankjærgaard (2011) defined a “fast” and a “slow” time-resolved signal and found different behaviour of these two for the IRSL and post-IR IRSL signals measured in the UV at elevated temperatures, and that the relative signal intensity between the fast and slow signal contribution changes.

Here we compare lifetimes obtained for the two IRSL signals measured in the blue using a post-IR_{50} $IRSL_{225}$ protocol. Figure 2 shows lifetimes of all samples obtained by fitting on- and off-time signals of the $IRSL_{50}$ and post-IR $IRSL_{225}$. Figs. 2A and B show a direct comparison of all measured lifetimes and their distribution around a 1:1 line, for the on- and off-times respectively. Especially at faster lifetimes and in the off-time signal, $IRSL_{50}$ and post-IR $IRSL_{225}$ yield similar results and even the slower signals show results scattered around the 1:1 line (Fig. 2 A, B). Sample-dependent lifetimes presented in Figs. 2C and D indicate variations in the presence of different lifetimes in the samples investigated. Further details regarding sample-to-sample variations are discussed qualitatively in section 3.2. However, what is also visible from Figs. 2C and D is that in some samples, some lifetimes only occur in either the $IRSL_{50}$ or the post-IR $IRSL_{225}$ signal (e.g. Lifetime 1 in the on-time of sample FSM-6). Such points are not visible from the diagrams in Figs. 2A and B. Despite these minor deviations and some observed variability, it

317 can be concluded that overall similar lifetimes can be obtained for all samples regardless of the IRSL
318 signal chosen.

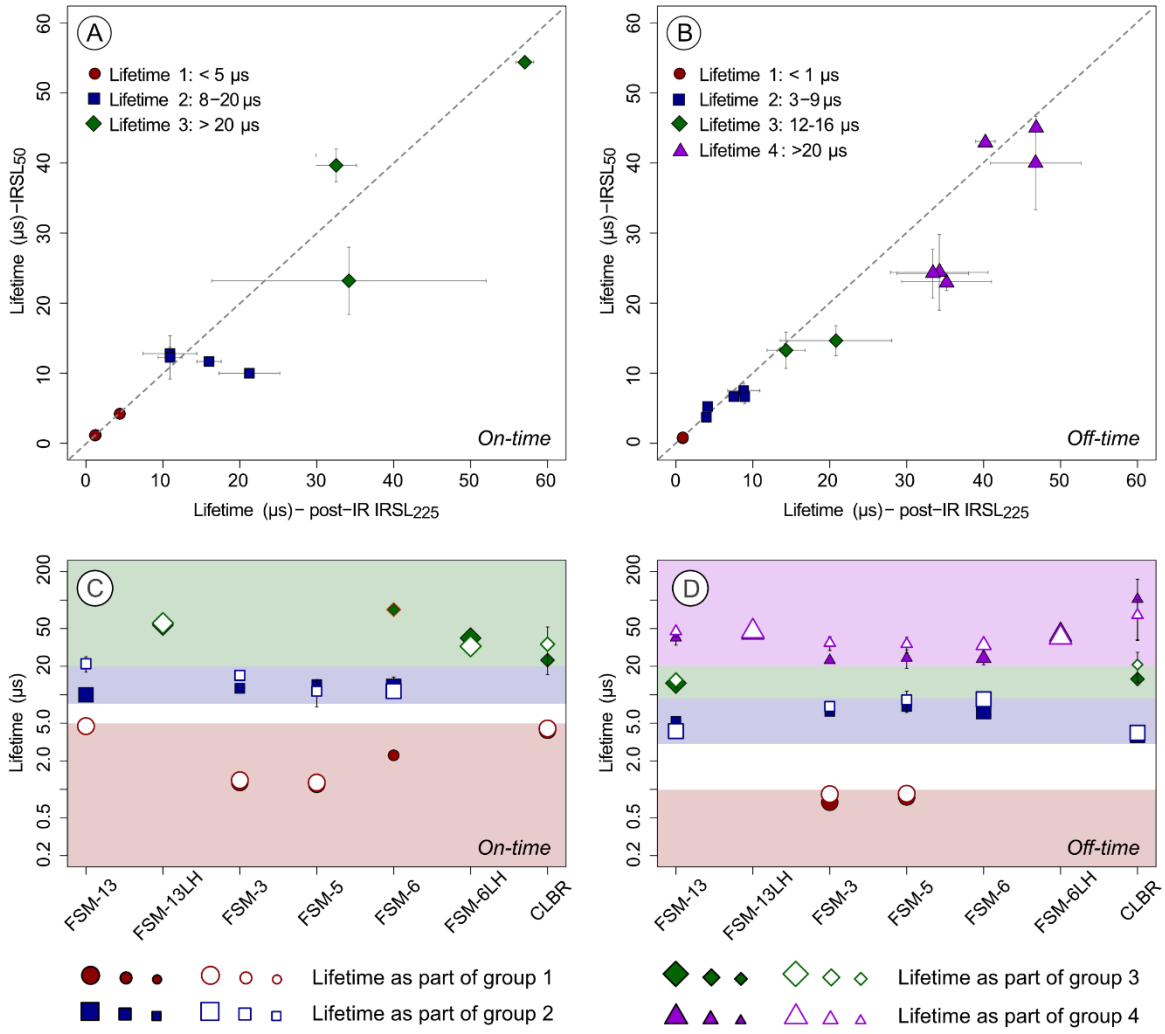

Fig. 2. Comparison of lifetimes obtained for the $IRSL_{50}$ and post-IR $IRSL_{225}$ signals for the on-time (A) and off-time (B) of the blue emission (50 Gy given dose). The dashed line in the graphs represent the one-to-one line. The data shown here is for all samples measured. The same data is shown in (C) and (D) where the fitted lifetime components are resolved for the individual samples. The data points in all figures represent the mean of three aliquots and their standard deviation. The diamond with red border (C) shows a lifetime, which only observed in one aliquot. The different sizes of the symbols in subfigures C and D indicate how prominent the component is within the given sample; the larger the symbol the more prominent is the component.

319

320 ***Dose dependency***

321 Ankjærgaard et al. (2009) compared time-resolved OSL (470 nm LED and 532 nm laser stimulated)
322 lifetimes measured in the UV for different feldspars following irradiation doses of 5 Gy and 1000 Gy,
323 dependent on sample brightness, and showed that lifetime determination is independent of the dose
324 administered. However, Ankjærgaard et al. (2009) did not explore IRSL or post-IR IRSL signals. Here we
325 show the results of a systematic investigation of potential lifetime-dependencies for the blue emission
326 ($IRSL_{50}$ and post-IR $IRSL_{225}$) for irradiation doses of 50 Gy, 200 Gy and 800 Gy (Fig. 3). The fitting results

presented in direct comparison for the different doses in Fig. 3 scatter around the one-to-one line, indicating independence of the lifetimes of the doses given and thus supporting earlier work by Ankjærgaard et al. (2009) for OSL of feldspars.

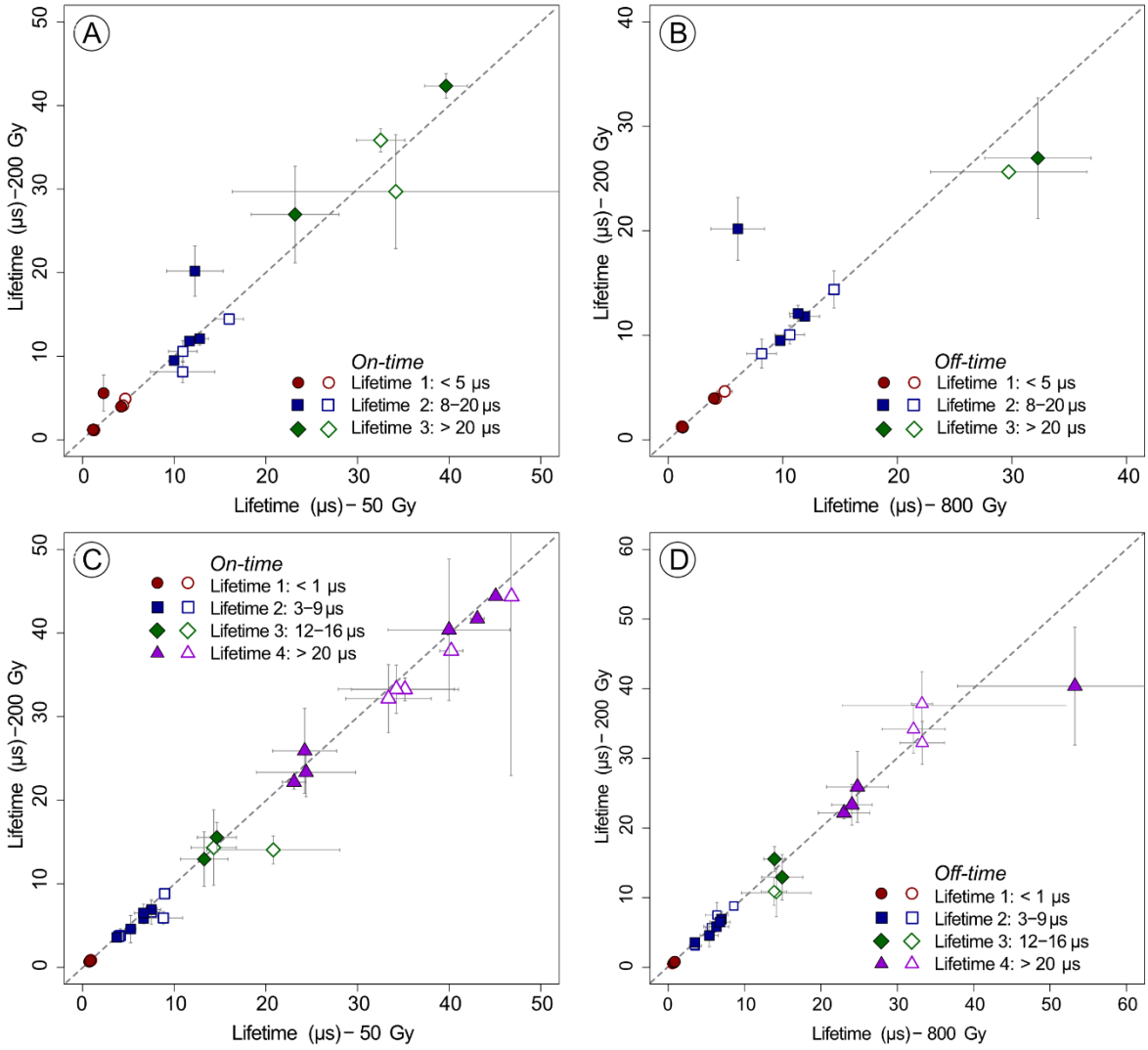

Fig. 3. Testing potential dose dependencies on the lifetimes of the $IRSL_{50}$ (filled symbols) and the post-IR $IRSL_{225}$ signal (open symbols) signal of the blue IRSL emission (on-time: A and B, off-time: C and D). Four doses were tested for this experiment, where the results of lifetimes obtained in response to 50 Gy are compared to 200 Gy (A and C) and 200 Gy are compared to 800 Gy (B and D).

Lifetimes compared to literature values

Measurements performed in this paper resulted in lifetimes spanning the following time scales: On-time: (1) < 5 μs, (2) 8-20 μs, (3) > 20 μs. Off-time: (1) < 1 μs, (2) 3-9 μs, (3) 12-16 μs, (4) > 20 μs. These lifetimes, obtained for the $IRSL_{50}$ and post-IR $IRSL_{225}$ signal, are in good agreement with previous work: Clark and Bailiff (1998) presented very fast lifetimes of different emissions measured for various chemically different feldspar samples using pulsed 850 nm laser stimulation. Their lifetimes range from a few ns to the μs-scale. Due to instrumental limitations, we are unable to detect lifetimes faster than

0.3 µs, but lifetimes measured on the µs-scale in this paper are similar to those obtained by Clark and Bailiff (1998). Using the sum of three exponential functions to describe the off-time decay, Tsukamoto et al. (2006) measured blue IRSL lifetimes of 0.61, 2.4 and 19 µs for a Na-feldspar sample (grain mixture) and 1.1, 4.3 and 19 µs for a K-feldspar sample (grain mixture). These values and the number of exponentials used to describe the decay are similar to the results obtained in the present study (cf. Fig. 2). Ankjærgaard et al. (2009) compared lifetimes of chemically different single crystal feldspars and feldspar grain mixtures. These authors observed the UV emission of 532 nm laser and 470 nm diode stimulated feldspars and enabled a comparison by using the sum of multiple first order exponentials for fitting their off-time signals. The feldspars investigated showed lifetimes for the UV emission on the µs-scale, with the fastest lifetimes (<0.1 µs) obtained through pulsed 532 nm laser stimulation. Longest lifetimes measured ranged from ~10 µs to <100 µs, and are thus within the range of lifetimes obtained in the present study, but it should be noted that stimulation and emission wavelengths differ from our study.

Excited state vs. recombination lifetime?

Here we compared lifetimes of different feldspars, measured using two different IRSL signals, obtained from different IRSL integration intervals, and after different irradiation doses. Figs. 2 and 3, and Fig. S2 showed that the lifetimes seem to be largely independent of the given dose, the signal integration interval and IRSL signal measured. This observation supports the excited state lifetime hypothesis if one assumes a random distribution of donor and acceptor pairs in a proximity model. However, the recombination lifetime might still be considered as a valid explanation, if the defect density is so high that changes to e.g. the number of populated defects through different doses might be so small that changes to the lifetime cannot be observed.

3.2 Sample-to-sample variations in the blue time-resolved $IRSL_{50}$ signal

We showed in section 3.1 that neither the on- nor the off-time of the blue IRSL signal depends on the IRSL signal integration interval, or the dose given. We also showed that the $IRSL_{50}$ signal and the post-IR $IRSL_{225}$ signal result in similar lifetimes. Thus, these findings support the excited state lifetime hypothesis, unless the defect density is too high to observe any potential changes of the populated defects and their effect on the lifetimes. In the following we investigate time-resolved IRSL (blue emission) of a suite of chemically and structurally well-constrained alkali feldspars for which Riedesel et al. (2021a, b) have demonstrated how their different compositions and structure impact the blue and infrared luminescence emissions and fading rates. This will enable us to study variations in time-resolved luminescence signals and their potential physical causes. Since no dependence on dose and IRSL signal investigated were found in the previous experiments all results shown in the following are based on the $IRSL_{50}$ signal which was recorded after a dose of 200 Gy. The discussion is based on

qualitative comparisons between samples, as we will make some statements regarding potential physical processes in feldspars. Except in cases where time-resolved signals can be fitted using a single exponential function, no quantitative assessments are made, to avoid confusion about the kinetic order of feldspar luminescence.

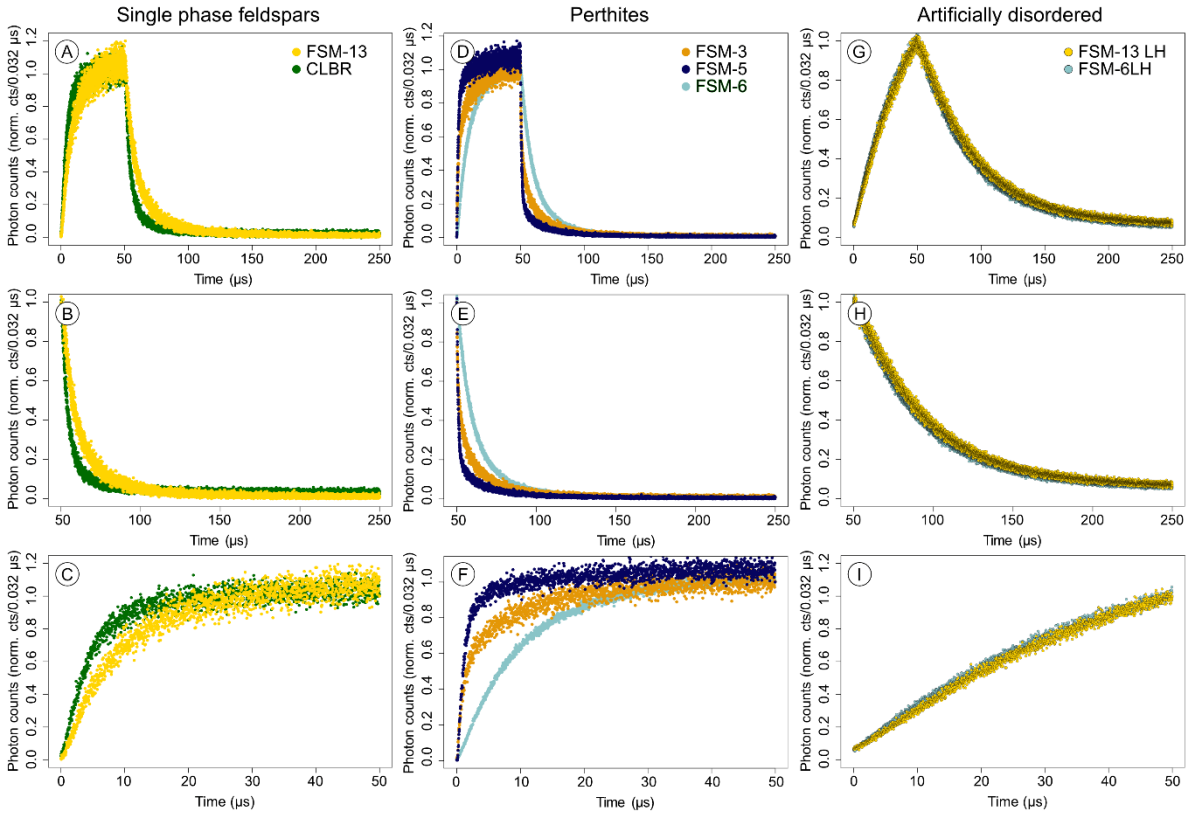

Fig. 4. Time-resolved $IRSL_{50}$ of the blue emission (200 Gy) for single phase feldspars, perthites and artificially disordered samples. A, D and G show the whole signals, B, E and H the off-time signal and C, F and I the on-time.

Figure 4 shows a comparison of blue time-resolved $IRSL_{50}$ signals obtained for the different samples. For the seven feldspars investigated we observed a range of different time-resolved luminescence signals. Whilst all samples show an on-time signal increase and an off-time decay on the µs-scale, there are subtle differences between samples. The fastest rise and decay can be found in macroperthite FSM-5 (Fig. 4D-F), followed by K-rich cryptoperthite FSM-3, where the short lifetime components appear to be dominating the shape. Perthitic sample FSM-6 and the two single phase feldspars microcline FSM-13 and albite CLBR show similar time-resolved signals, although CLBR shows faster signal increase and decay compared to FSM-13 (Fig. 4A-C). The slowest rise and decay of the time-resolved IRSL signal can be found in the two artificially disordered feldspars FSM-13LH and FSM-6LH (Fig. 4G-I), where the longer lifetime components appear to be dominating the shape. A direct comparison between the artificially disordered samples FSM-13LH and FSM-6LH and their ordered counterparts is shown in Figure 5. When comparing the artificially disordered samples FSM-13LH and

FSM-6LH it is evident that the two samples show very similar on- and off-time signal behaviour, with samples FSM-6LH showing only slightly faster signals. Fitting of the time-resolved luminescence signals of these two artificially disordered samples was possible by using a single exponential function plus a constant background signal (i.e. k in eq. 2) and lifetimes obtained are around ~45 µs.

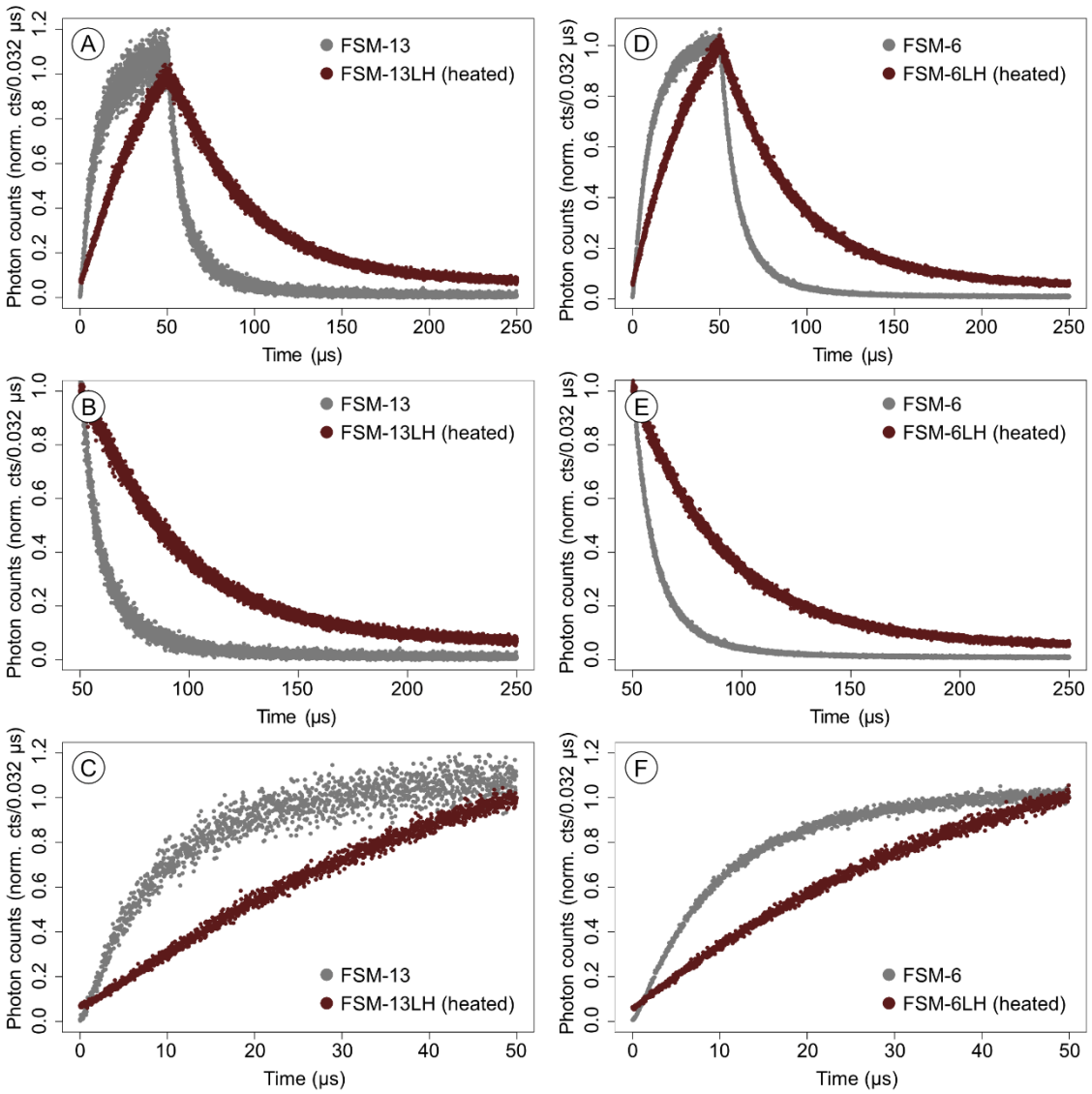

Fig. 5. Time resolved signals of the blue $IRSL_{50}$ emissions (200 Gy) of unheated and heated sample pairs FSM-13 and FSM-13LH (A, B, C) and FSM-6 and FSM-6LH (D, E, F).

This slow rise and decay and the lifetimes obtained from fitting using a single exponential function are similar to results obtained for quartz elsewhere (e.g. Bailiff, 2000; Chithambo 2003; 2007). One other feature of quartz time-resolved luminescence signals is a significant decrease in lifetime with increasing stimulation temperature, which has been associated with thermal quenching (Bailiff, 2000; Chithambo, 2003). Bailiff (2000) observed a decrease in the decay lifetime of synthetic quartz from~40 µs to 8 µs, when increasing the stimulation temperature from room temperature to 210 °C. These observations are supported by similar experiments made by Chithambo (2003) on natural sand-sized

quartz. To test potential influence from thermal quenching on lifetimes and time-resolved luminescence signals of artificially disordered feldspars, we measured time-resolved IRSL signals at different stimulation temperatures. The signals were recorded using the protocol described in Table 2. We varied the stimulation temperature of the post-IR IRSL signal (step 5 in Table 2) from 50 °C to 225 °C in 25 °C steps. In contrast to observations made on quartz, our artificially disordered feldspars do not show thermal quenching (cf. Fig. 6) and lifetimes measured remain at a constant level around ~45 µs. Thus, we conclude that artificial disordering influences the lifetime of the blue emission, however, the resulting emission and related processes seem to differ from what has been observed for quartz, and thus do not show any thermal quenching effects.

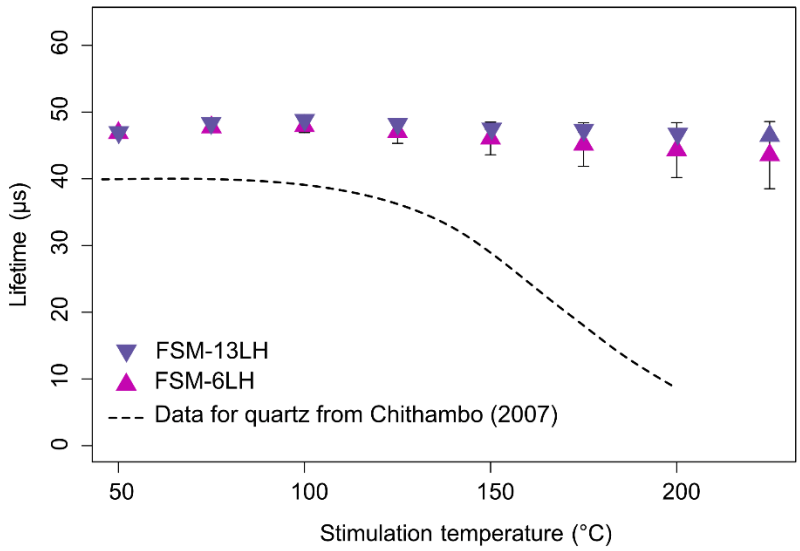

Fig. 6. Effect of varying the stimulation temperature of the post-IR IRSL signal on the lifetimes of the second IRSL signal in the post-IR_{50} $IRSL_{50\text{-}225\ °C}$ protocol on disordered (heated) samples FSM-13LH and FSM-6LH. The lifetimes are compared to data obtained from quartz (Chithambo, 2007). Data points from this study represent the average and standard deviation of measurements of three aliquots.

The sample-to-sample variations in rise and decay of the time-resolved IRSL signals are striking, particularly showcasing the changes observed for the ordered and disordered samples pairs. Whilst we observe these variations in time-resolved signals, we so far cannot explain what causes these. However, these samples have been investigated previously and thus some information regarding their luminescence characteristics are known, enabling potential links between existing information and the newly gathered time-resolved results.

When comparing TL emission spectra and fading rates of the same single-phase feldspars and perthites as explored in the present study, Riedesel et al. (2021a) observed differences in emission intensities and fading rates of the samples investigated. Whilst single-phase feldspars (microcline and albite) only showed weak blue luminescence and no fading, cryptoperthites were characterised to have intense and broad blue emissions and fading rates ranging from ~2 to ~7 %/decade. Macroperthites exhibited

the highest fading rates with up to 12 %/decade. Riedesel et al. (2021a) found that these observations support a location for the defect responsible for the blue emission on Al-O-Al bridges (cf. Finch and Klein, 1999). The data presented by Riedesel et al. (2021a) suggests that potentially higher densities of these defects can be found along the interfaces in perthites. When comparing time-resolved IRSL measurements of single-phase feldspars, albite (CLBR) and microcline (FSM-13), and perthites (FSM-3, FSM-5 and FSM-6), slightly slower time-resolved IRSL on-time rise and off-time signal decays can be found for single-phase feldspars compared to perthites consisting of albite and microcline (cf. FSM-3 and FSM-5, Fig. 4A-C compared with Fig. 4D-F). Contrastingly, perthite FSM-6 shows time-resolved IRSL signals similar to the two single-phase feldspars investigated. Interestingly FSM-6, a perthite, consists of orthoclase and albite, indicating a slightly more disordered structure in FSM-6 compared to the other two perthites.

Riedesel et al. (2021a) also compared TL emission spectra and fading rates of the same ordered and disordered sample pairs as investigated here. They found that the blue luminescence emission intensity and the IRSL fading rate increased with framework disorder. This was interpreted as the result of an increase in recombination centre density due to framework disorder. A denser defect population would, if the recombination lifetime hypothesis holds true, result in a faster time-resolved luminescence signal. However, the contrary is observed here (cf. Fig. 5), with disordered feldspars (FSM-13LH, FSM-6LH) showing the slowest time-resolved signals. This potentially indicates a change in the blue luminescence centre properties and thus a change to the excited state lifetime of this luminescence centre.

Whilst large differences in fading rate and blue luminescence emission intensity were found across different feldspars, electron trapping centres, understood to be involved in feldspar IRSL (e.g. Prasad et al., 2017; Kumar et al. 2018), seem to be largely independent of changes to the sample chemistry or structure (Riedesel et al., 2019, 2021b). Riedesel et al. (2019, 2021b) showed that the electron trapping centre depth as well as emissions related to trapping and retrapping at electron trapping centres are similar across the alkali feldspar group.

If the electron trapping centres are independent of the sample's chemistry or structural state, then changes in lifetime of the blue luminescence emission in ordered and disordered sample pairs and across the chemical range of alkali feldspars, are either related to changes in the blue luminescence centre itself or to parts of the crystal unrelated to electron trapping centres. Ankjærgaard and Jain (2010) and Jain and Ankjærgaard (2011) suggested that the slower part of the TR decay could result from recombination via the band-tail states. Pagonis et al. (2012) further investigated this hypothesis by exploring time-resolved IRSL signals of four feldspar museum specimens. Pagonis et al. (2012) applied a fitting approach which combined a single exponential and a stretched exponential function,

where the authors related the results of the stretched exponential to the band-tail states. The observed increase in time-resolved IRSL lifetime with increasing disorder of the framework in this paper could be related to a higher density of band-tail states or a wider band-tail due to disorder of the crystal. A wider or denser sub-conduction band tail could potentially result in an increased transport of charge via these states – resulting in slower recombination processes than would be expected for excited state tunnelling (cf. Jain and Ankjærgaard, 2011).

Additionally, Tsukamoto et al. (2006) found that longer lifetime components (> 20 μs) were more stable in laboratory storage experiments. When comparing fading results of the samples investigated here (cf. Riedesel et al., 2021a) then a positive relationship between increasing fading rate and increasing longer lifetime components can be found for the ordered and disordered sample pairs (FSM-13/FSM-13LH and FSM-6/FSM-6LH). However, macroperthite FSM-5 was amongst the samples showing the highest fading, with an $IRSL_{50}$ fading rate of ~9 %/decade, but it also shows the fastest on- and off-time signals (cf. Fig. 4D, E, F) amongst the samples presented here. Thus, based on the present data set, no clear relationship between fading rate and time-resolved signal rise and decay can be established.

4 Yellow-green time-resolved IRSL emission – Results and Discussion

The yellow-green emission is rarely used in luminescence dating applications, however, it has been identified as a common emission in many plagioclase feldspars (e.g. Geake et al., 1971, 1973, 1977; Telfer and Walker, 1978), and was also recorded in microcline samples (c.f. Rendell and Clarke, 1997; Riedesel et al., 2021a). Whilst being present as a distinct emission in some samples, the broad emission recorded for perthites often spans from the blue into the yellow wavelength region (cf. Riedesel et al., 2021a) and might thus include this emission. Two potential defects have been proposed for causing this emission: (i) Mn^{2+} substituting for Ca^{2+} on M sites (e.g. Geake et al., 1971, 1973, 1977; Telfer and Walker, 1978) or (ii) Mn^{2+} substituting for Al^{3+} on T sites (Telfer and Walker, 1978; Kirsh et al., 1987; Clark and Bailiff, 1998). In the following we show the recorded time-resolved IRSL signals for the yellow-green emission and the sample-to-sample variations we observed for this emission. The results shown in this section are based on time-resolved measurements of the $IRSL_{50}$ signal, measured after an irradiation dose of 200 Gy (or 400 Gy, in case of FSM-5 and FSM-6).

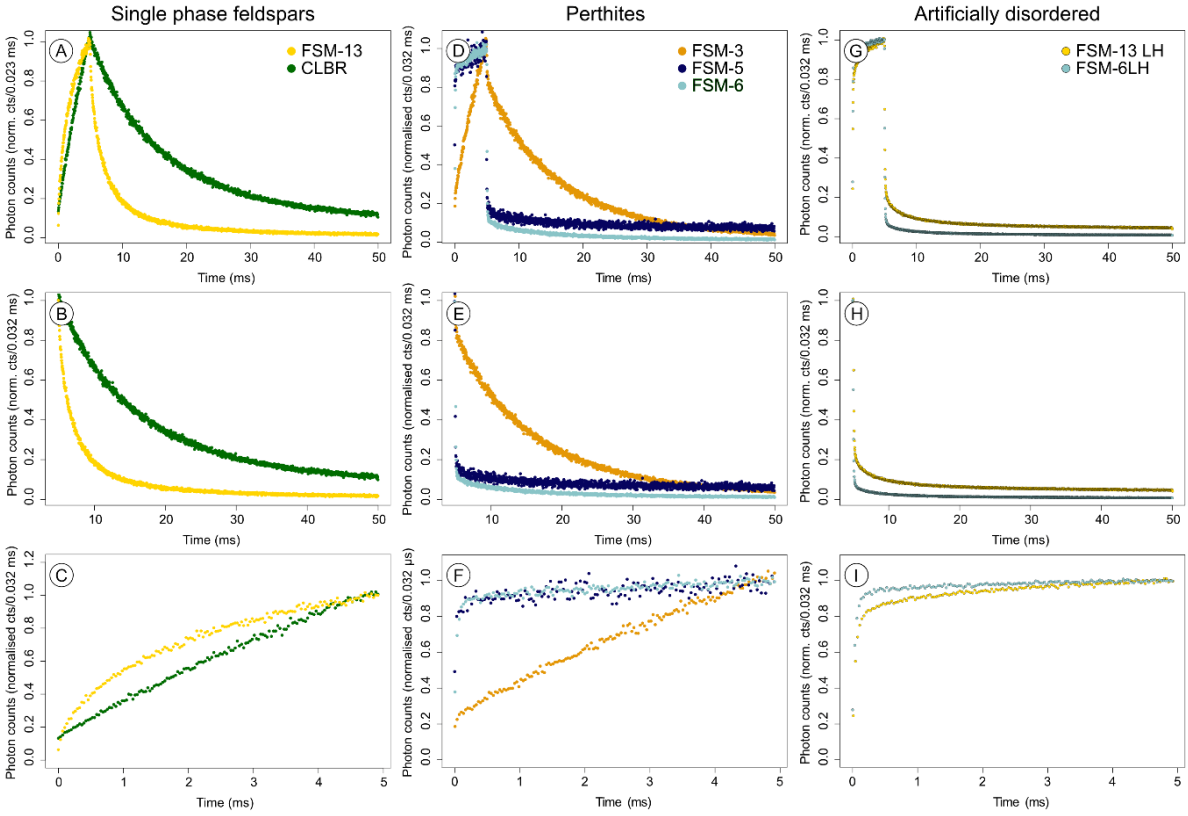

Fig. 7. Time-resolved $IRSL_{50}$ of the yellow-green emission for single phase feldspars, perthites and artificially disordered samples. The signals were recorded after an irradiation dose of 200 Gy (400 Gy in case of FSM-5 and FSM-6). A, D and G show the whole signals, B, E and H the off-time signal and C, F and I the on-time.

For all samples we observed time-resolved IRSL signals on the ms-scale (Fig. 7), which is much slower compared to most of the observations made for the blue emission (Fig. 4). However, the different samples contain varying proportions of the slower part of the TR signal. Especially in perthitic and disordered samples the yellow-green emission is dominated by a very fast component, visible by the sharp increase at the beginning of the on-time and the sharp decrease at the start of the off-time (cf. Figs. 7 D-I). TR on-and off-time signals of single-phase feldspars FSM-13 and CLBR and perthite FSM-3 are significantly slower compared to the other samples (cf. Fig. 7A-C, D-F).

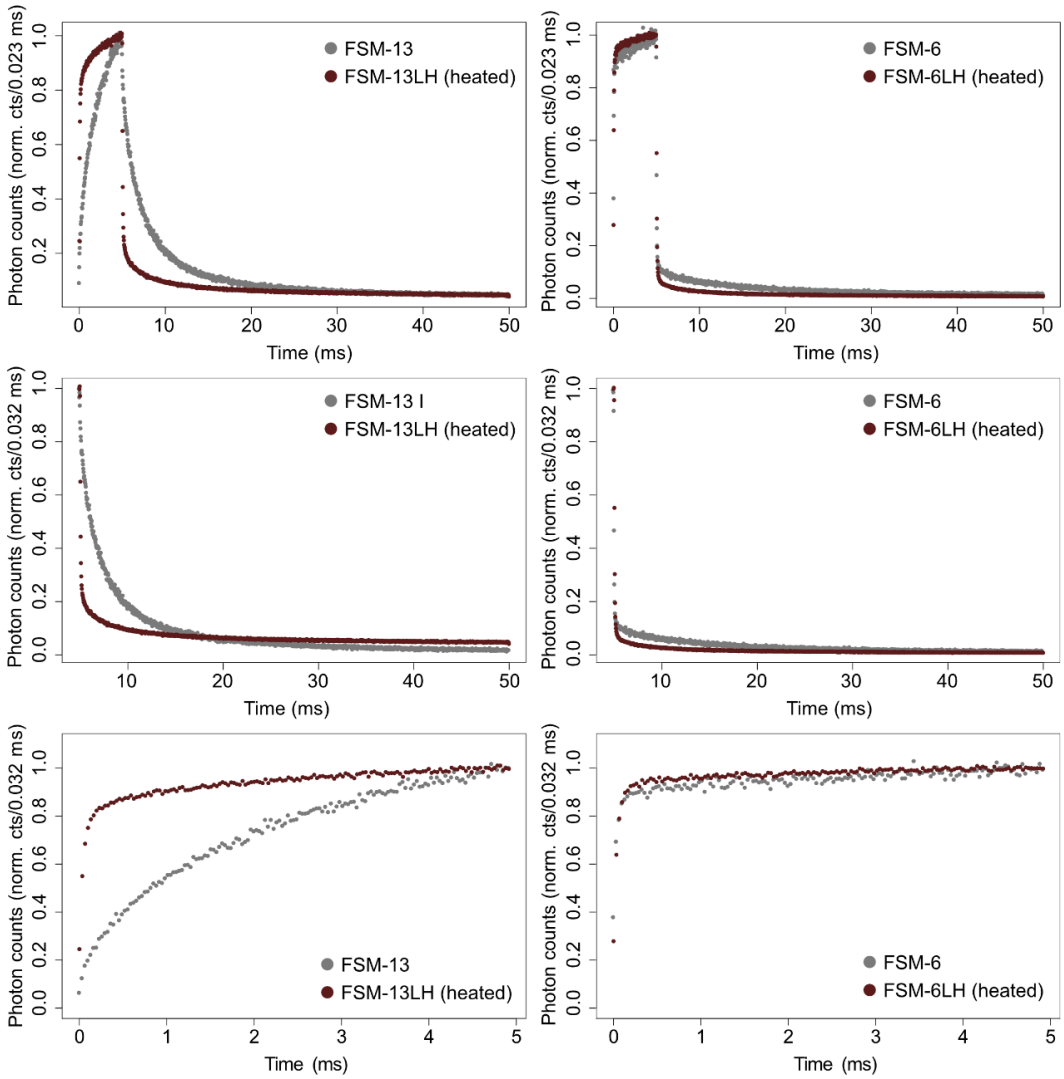

Fig. 8. Time resolved signals of the yellow-green $IRSL_{50}$ emissions of unheated and heated sample pairs FSM-13 andFSM-13LH (heated) (A, B, C) and FSM-6 andFSM-6LH (heated) (D, E, F).

A comparison of the ordered and disordered sample pairs reveals that the yellow-green emission becomes faster during on- and off-times when the sample is disordered (Fig. 8). The effect is more visible in the case of FSM-13 and FSM-13LH, compared to FSM-6 and FSM-6LH. However, from TL emission spectra it becomes apparent that disordering results in a significant increase in blue TL emission intensity (Riedesel et al., 2021a). This could potentially result in breakthrough of this strong blue emission into the emission window we used to record the yellow-green emission (cf. transmission of the filter combination on a log-scale in Fig. S1B). This might also explain the fast initial rise and decay in samples FSM-3 and FSM-5. Alternatively, the fast signals recorded for the yellow-green emission could originate from the defect being located on a tetrahedral site, as previously suggested by Clark and Bailiff (1998). These authors observed very fast lifetimes for the yellow-green emission, even on the ns-scale, when fitting their time-resolved signals.

Whilst we proposed a potential influence of band-tail states as the explanation for longer lifetimes of the blue emission in disordered samples, this hypothesis would not hold in case of the yellow-green emission, as the slowest signal rise and decay is found in ordered end member samples.

Observing significant differences in the time scale of signal rise and decay of different samples investigated here could indicate that the emission indeed results from two different defect types. Long lifetimes obtained here for single-phase microcline FSM-13 and albite CLBR suggest a metal ion site defect as source of the yellow-green emission, even in alkali feldspars, supporting the Mn^{2+} substituting for Ca^{2+} on M site hypothesis by e.g. Telfer and Walker (1978). In this case, a spin-forbidden transition would explain the lifetimes on the ms-scale. However, short lifetimes (µs-scale) would be expected for a defect resulting from Mn^{2+} substituting for Al^{3+} on T sites (cf. Clark and Bailiff, 1998). In this case the defect responsible for the yellow-green emission would be a lattice stabilising hole centre on Si^{4+}-O^{-}-Mn^{2+}, as the hole centre on the O ion would help in charge neutralisation, due to the introduced imbalance by Mn^{2+} substituting for Al^{3+} (Telfer and Walker, 1978; Kirsh et al., 1987). If this type of defect is indeed present in our samples, then one would expect that framework disorder influences the lifetime of this signal, as is also shown in Fig. 8. Unfortunately, we cannot completely rule out any influence of breakthrough of the blue emission, so no definite answer can be given here. However, it is striking that the strong yellow-green emission can be found in the single-phase microcline, a K-rich alkali feldspar end member, which also shows on-time increase and off-time decrease on similar time-scales as seen for the albite specimen. This could indicate that whatever the type of defect, it is not restricted to plagioclase feldspars and might thus not be Mn^{2+} substituting for Ca^{2+} on M sites.

5 Conclusions

In this paper we presented time-resolved infrared stimulated luminescence signals measured for a range of single crystal alkali feldspars, including K- and Na-feldspar end members (microcline and albite, both single phase), for the blue emission (~410 nm) and the yellow-green emission (~550 nm) using a post-IR_{50} $IRSL_{225}$ protocol. The timescale on which the blue and the yellow-green emissions occur differ significantly; the blue signal on the µs-scale, and the yellow-green emission on the ms-scale. For each emission the lifetimes are independent of the signal integration interval, the IRSL signal investigated, and the dose given.

For the blue emission there is a slight difference in decay time scale between single-phase feldspars and perthites, however more significant differences are observed when the feldspars are artificially disordered. Our new observations show that artificially disordering the framework increases the rise and decay time of the on- and off-time, and that the signals can now be described using a single exponential fit. The lifetimes obtained from the disordered feldspars are similar to those measured for

quartz elsewhere (c.f. Bailiff 2000, Chithambo 2003), but unlike for quartz the time-resolved signals here do not show any thermal quenching. The longer lifetimes observed for disordered feldspars may have two causes: 1. Disordering of the Si,Al-framework could result in a change of the blue recombination centre, resulting in longer excited state lifetimes of the defect itself. 2. Increased disorder of the lattice could cause changes to the band-tail state width or density. This in turn might increase the likelihood of recombination occurring via the band-tail states, resulting in longer recombination lifetimes (c.f. Jain and Ankjærgaard, 2011; Pagonis et al., 2012).

Time-resolved signals of the yellow-green emission vary between samples, with single-phase microcline and albite specimens showing the slowest signals. These slow time scales could indicate a spin-forbidden transition, as has been proposed for a defect resulting from Mn^{2+} substituting for Ca^{2+} on M sites. However, the Ca content of the microcline specimen is negligible and the Mn content so low that it could not be detected. In contrast to slow signals in the single-phase samples, perthitic and disordered samples show a large proportion of a fast signal decay in the off-time, before a slow component describes the remaining part of the time-resolved signal. The fast signal could either indicate a different type of defect for this emission or, alternatively, it could be an artefact resulting from breakthrough of the blue emission. This needs further investigation in future measurements.

The data in this paper shows the potential for using time-resolved IRSL with emission detected in the blue to gain information on the structural state of the feldspar investigated and thus helping in understanding variations in luminescence properties across a range of chemically and structurally different feldspars.

Acknowledgements

Initial time-resolved luminescence measurements, which formed the basis for the research presented in this paper, were performed during SR's PhD at Aberystwyth University. SR's PhD research was funded through an AberDoc PhD scholarship by Aberystwyth University. We would like to thank Hollie Wynne (Aberystwyth University) for preparing the aliquots for all measurements, so that SR could run the experiments remotely during the Covid-19 pandemic. We would like to thank Anthony M.T. Bell (Sheffield Hallam University) for performing XRF and XRD measurements, characterising the feldspar samples used in this study. We would like to thank two anonymous reviewers for their constructive feedback.

568 **References**

569 Ankjærgaard, C., Jain, M., Kalchgruber, R., Lapp, T., Klein, D., McKeever, S.W.S., Murray, A.S.,
570 Morthekai, P., 2009. Further investigations into pulsed optically stimulated luminescence from
571 feldspars using blue and green light. Radiation Measurements 44, 576-581.

572 Ankjærgaard, C., Jain, M., 2010. Optically stimulated phosphorescence in orthoclase feldspar over the
573 millisecond to second timescale. Journal of Luminescence 130, 2346–2355.

574 Bailiff, I.K., 2000. Characteristics of time-resolved luminescence in quartz. Radiation Measurements 32,
575 401-405.

576 Bates, D. M. and DebRoy, S., 2018. nls function—nonlinear least squares R Core Team and contributors
577 worldwide, 2018. The R stats package version 3.5.0 .

578 Buylaert, J.-P., Jain, M., Murray, A.S., Thomsen, K.J., Thiel, C., Sohbati, R., 2012. A robust feldspar
579 luminescence dating method for Middle and Late Pleistocene sediments. Boreas 41, 435-451.

580 Cassadanne, J.P., Roditi, M., 1996. The location, geology and mineralogy of gem tourmalines in Brazil.
581 Journal of Gemmology 25 (4), 263–298.

582 Chithambo, M.L., 2003. Dependence of the thermal influence on luminescence lifetimes from quartz
583 on the duration of optical stimulation. Radiation Measurements 37, 167-175.

584 Chithambo, M.L., 2007. The analysis of time-resolved optically stimulated luminescence: II. Computer
585 simulations and experimental results. Journal of Physics D: Applied Physics 40, 1880-1889.

586 Clark, R.J., Bailiff, I.K., Tooley, M.J., 1997. A preliminary study of time-resolved luminescence in some
587 feldspars. Radiation Measurements 27, 211-220.

588 Clark, R.J., Bailiff, I.K., 1998. Fast time-resolved luminescence emission spectroscopy in some feldspars.
589 Radiation Measurements 29, 553-560.

590 Cunningham, G.J., 1981. Petrology and geochemistry of Lewisian pegmatites and granites, N.W.,
591 Scotland. PhD thesis, Imperial Collage London, United Kingdom.

592 Deer, W.A., Howie, R.A., Zussman, J., 2013. An Introduction to the Rock-Forming Minerals, third ed.
593 Mineralogical Society of Great Britain and Ireland.

594 Duller, G.A.T., 1997. Behavioural studies of stimulated luminescence from feldspars. Radiation
595 Measurements 27, 663-694.

596 Finch, A.A., Klein, J., 1999. The cause and petrological significance of cathodoluminescence emissions
597 from alkali feldspars. Contributions to Mineralogy and Petrology 135, 234-243.

598 Geake, J.E., Walker, G., Mills, A.A., Garlick, G.F.J., 1971. Luminescence of Apollo lunar samples.
599 Proceedings of the Second Lunar Science Conference 3, 2265-2275.

600 Geake, J.E., Walker, G., Telfer, D.J., Mills, A.A., Garlick, G.F.J., 1973. Luminescence of lunar, terrestrial,
601 and synthesized plagioclase caused by Mn^{2+} and Fe^{3+}. Proceedings of the Fourth Lunar Science
602 Conference 4, 3181-3189.

603 Geake, J.E., Walker, G., Telfer, D.J., Mills, A.A., 1977. The cause and significance of luminescence in
604 lunar plagioclase. Philosophical transactions of the Royal Society A 285, 403-408.

605 Godfrey-Smith, D.I., Huntley, D.J., Chen, W.-H., 1988. Optical dating studies of quartz and feldspar
606 sediment extracts. Quaternary Science Reviews 7, 373-380.

607 Hütt, G., Jaek, I., Tchonka, J., 1988. Optical Dating: K-feldspars optical response stimulation spectra.
608 Quaternary Science Reviews 7, 381-385.

609 Huntley, D.J., 2006. An explanation of the power-law decay of luminescence. Journal of Physics:
610 Condensed Matter 18, 1359-1365.

611 Jain, M., Ankjærgaard, C., 2011. Towards a non-fading signal in feldspar: Insight into charge transport
612 and tunnelling from time-resolved optically stimulated luminescence. Radiation Measurements 46,
613 292-309.

614 Jain, M., Guralnik, B., Andersen, M.T., 2012. Stimulated luminescence emission from localized
615 recombination in randomly distributed defects. Journal of Physics: Condensed Matter 24, 385402.

616 Kirsh, Y., Shoval, S., Townsend, P.D., 1987. Kinetics and emission spectra of thermoluminescence in the
617 feldspars albite and microcline. Physica Status Solidi 101, 253-262.

618 Kumar, R., Kook, M., Murray, A.S., Jain, M., 2018. Towards direct measurement of electrons in
619 metastable states in K-feldspar: Do infrared-photoluminescence and radioluminescence probe the
620 same trap? Radiation Measurements 120, 7-13.

621 Lapp, T., Jain, M., Ankjærgaard, C., Pritzel, L., 2009. Development of pulsed stimulation and Photon
622 Timer attachment to the Risø TL/OSL reader. Radiation Measurements 44, 571-575.

623 Lapp, T., Kook, M., Murray, A.S., Thomsen, K.J., Buylaert, J.P. and Jain, M., 2015. A new luminescence
624 detection and stimulation head for the Risø TL/OSL reader. Radiation Measurements 81, 178-184.

625 Pagonis, V., Morthekai, P., Singhvi, A.K., Thomas, J., Balaram, V., Kitis, G., Chen, R., 2012. Time-resolved
626 infrared stimulated luminescence signals in feldspars: Analysis based on exponential and stretched
627 exponential functions. Journal of Luminescence 132, 2330-2340.

628 Pagonis, V., Ankjærgaard, C., Jain, M., Chithambo, M.L., 2016. Quantitative analysis of time-resolved
629 infrared stimulated luminescence in feldspars. Physica B 497, 78-85.

630 Prasad, A.K., Lapp, T., Kook, M., Jain, M., 2016. Probing luminescence centres in Na rich feldspar.
631 Radiation Measurements 90, 292-297.

632 Prasad, A.K., Poolton, N.R.J., Kook, M., Jain, M., 2017. Optical dating in a new light: A direct, non-
633 destructive probe of trapped electrons. Scientific Reports 7: 12097.

634 Rendell, H.M., Clarke, M.L., 1997. Thermoluminescence, radioluminescence and cathodoluminescence
635 spectra of alkali feldspars. Radiation Measurements 27, 263-272.

636 Riedesel, S., King, G.E., Prasad, A.K., Kumar, R., Finch, A.A., Jain, M., 2019. Optical determination of the
637 width of the band-tail states, and the excited and ground state energies of the principal dosimetric
638 trap in feldspar. Radiation Measurements 125, 40-51.

639 Riedesel, S., Bell, A.M.T., Duller, G.A.T., Finch, A.A., Jain, M., King, G.E., Pearce, N.J., Roberts, H.M.,
640 2021a. Exploring sources of variation in thermoluminescence emissions and anomalous fading in alkali
641 feldspars. Radiation Measurements 141, 106541.

642 Riedesel, S., Kumar, R., Duller, G.A.T., Roberts, H.M., Bell, A.M.T., Jain, M., 2021b. Site-selective
643 characterisation of electron trapping centres in relation to chemistry, structural state and mineral
644 phases present in single crystal alkali feldspars. Journal of Physics D: Applied Physics 54, 385107.

645 Sanderson, D.C.W., Clark, R.J., 1994. Pulsed photostimulated luminescence of alkali feldspars.
646 Radiation Measurements 23, 633-639.

647 Shi, L., Huang, Y., Seo, H. J., 2010. Emission red shift and unusual band narrowing of Mn^{2+} in $NaCaPO_4$
648 phosphor. Journal of Physics and Chemistry A 114, 6927-6934.

649 Telfer, D.J., Walker, G., 1978. Ligand field bands of Mn2+ and Fe3+ luminescence centres and their site
650 occupancy in plagioclase feldspars. Modern Geology 6, 199-210.

651 Thomsen, K.J., Murray, A.S., Jain, M., Bøtter-Jensen, L., 2008. Laboratory fading rates of various
652 luminescence signals from feldspar-rich sediment extract. Radiation Measurements 43, 1474-1486.

653 Tsukamoto, S., Denby, P.M., Murray, A.S., Bøtter-Jensen, L., 2006. Time-resolved luminescence from
654 feldspars: New insights into fading. Radiation Measurements 41, 790-795.

655 Tsukamoto, S., Murray, A.S., Ankjærgaard, C., Jain, M., Lapp, T., 2010. Charge recombination processes
656 in minerals studied using optically stimulated luminescence and time-resolved exo-electrons. Journal
657 of Physics D: Applied Physics 43, 325502.

658 Ussher, W.A.E., Barrow, G., McAlister, D.A., 1909. The Geology of the country around Bodmin and St.
659 Austell. Memoirs of the Geological Survey England and Wales – Explanation of Sheet 347.

660

Supplementary Material

Time-resolved infrared stimulated luminescence of the blue and yellow-green emissions – insights into charge recombination in chemically and structurally different alkali feldspars

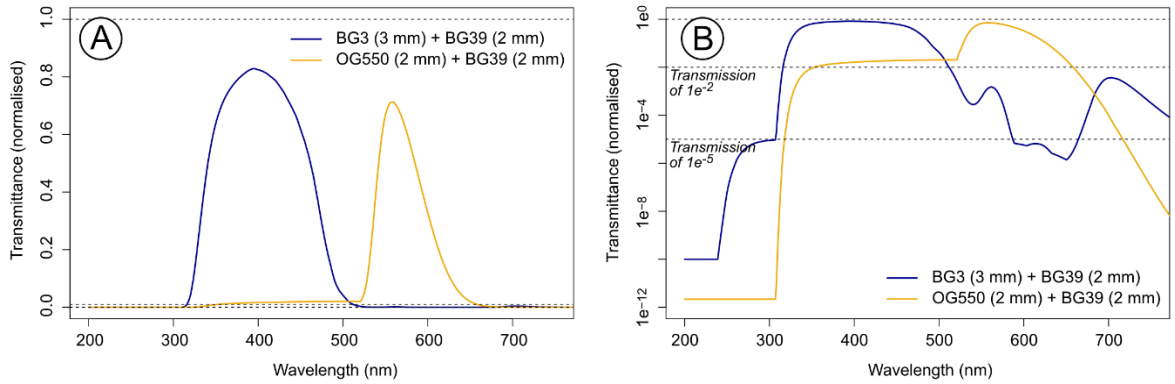

Fig. S1: Transmissions of filter combination used in this paper, with transmissions visualised on a linear (A) and on a logarithmic (B) scale.

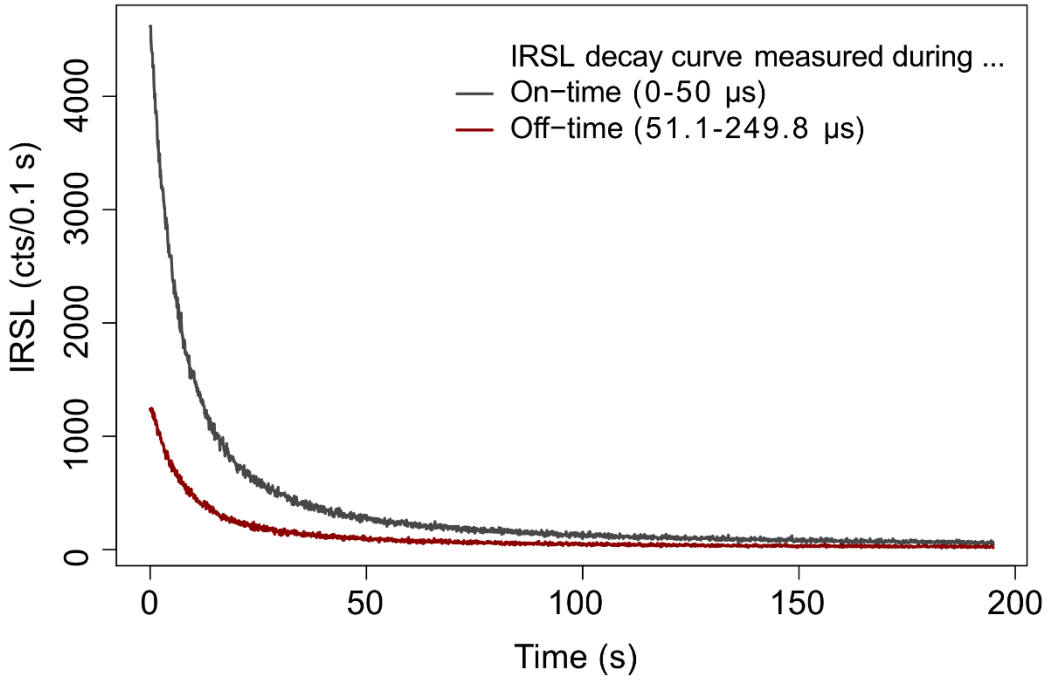

Fig. S2: $IRSL_{50}$ decay curves of sample FSM-13 measured during the on- (0-50 µs, grey curve) and off-times (51.1-249.8 µs, red curve) of the time-resolved luminescence measurements recorded in the blue emission window.

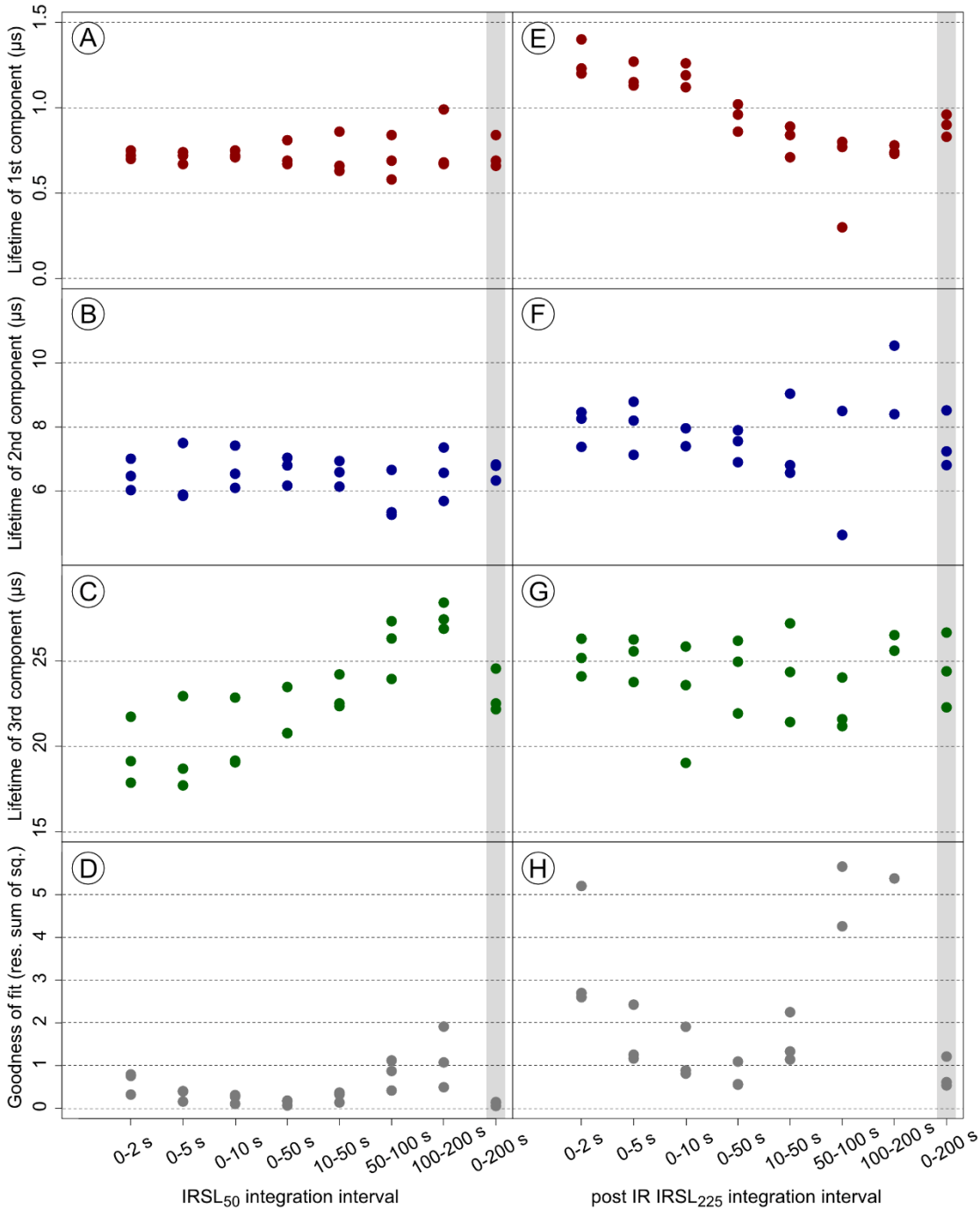

Fig. S3. Lifetimes and goodness of fit defined by the square sum of residuals for different integration time intervals for sample FSM-3. The data shown here is for the off-time signal of the blue emission and the two signals measured using the post-IR$_{50}$ IRSL$_{225}$ protocol, with results for the IRSL$_{50}$ signal in the left panels (A-D) and for the post-IR IRSL$_{225}$ on the right (E-H). The individual points show results for three aliquots measured.

668

669

*Table S1a: Lifetimes for the **blue IRSL$_{50}$** emission recorded in the **on-time** of the pulsed IRSL signal. I_i is the normalised intensity of the fitted lifetime τ_i (μs), k is a constant linear background. All values displayed are the average of three aliquots and the standard deviation. The data was normalised to the last data point of the on-time.*

Sample ID	Dose (Gy)	I_1	τ_1	I_2	τ_2	I_3	τ_3	I_4	τ_4	k	residual sum of squares
FSM-13	50			1.00 ± 0.05	9.99 ± 0.27					0.01 ± 0.01	2.43 ± 0.72
FSM-13LH	50					1.56 ± 0.04	54.38 ± 0.76			0.04 ± 0.00	0.29 ± 0.07
FSM-3	50	0.61 ± 0.09	1.18 ± 0.18	0.42 ± 0.08	11.67 ± 0.22					-0.03 ± 0.01	0.50 ± 0.21
FSM-5	50	0.96 ± 0.05	1.13 ± 0.01	0.18 ± 0.03	12.79 ± 0.94					-0.10 ± 0.00	1.38 ± 0.47
FSM-6	50	0.29 ± 0.00	2.29 ± 0.19	0.76 ± 0.09	12.26 ± 3.09	0.25[a]	79.39[a]			0.00 ± 0.00	1.42 ± 0.90
FSM-6LH	50					1.33 ± 0.03	39.66 ± 2.33			0.05 ± 0.00	0.06 ± 0.02
CLBR	50	0.88 ± 0.05	4.21 ± 0.54			0.18 ± 0.09	23.19 ± 4.80			0.01 ± 0.06	0.42 ± 0.18
FSM-13	200			0.92 ± 0.05	9.49 ± 0.24					0.02 ± 0.00	3.75 ± 0.99
FSM-13LH	200					1.60 ± 0.05	53.26 ± 1.00			0.04 ± 0.00	0.55 ± 0.18
FSM-3	200	0.60 ± 0.09	1.18 ± 0.18	0.43 ± 0.07	11.81 ± 0.10					-0.02 ± 0.01	1.21 ± 0.36
FSM-5	200	0.76 ± 0.06	1.22 ± 0.04	0.26 ± 0.02	12.09 ± 0.77					-0.08 ± 0.01	3.00 ± 0.98
FSM-6	200	0.57 ± 0.19	5.58 ± 2.15	0.53 ± 0.19	20.19 ± 3.00					0.01 ± 0.02	3.72 ± 2.81
FSM-6LH	200					1.39 ± 0.03	42.34 ± 1.46			0.05 ± 0.00	0.44 ± 0.37
CLBR	200	0.91 ± 0.08	3.97 ± 0.19			0.17 ± 0.07	26.96 ± 5.78			-0.03 ± 0.01	1.15 ± 0.56
FSM-13	800			1.01 ± 0.05	9.77 ± 0.27					0.01 ± 0.01	6.46 ± 2.67
FSM-13LH	800	*Not measured due to very high signal intensities saturating the PMT despite adding an ND 2.0 filter.*									
FSM-3	800	0.54 ± 0.04	1.28 ± 0.46	0.50 ± 0.06	11.93 ± 1.29					0.00 ± 0.01	3.40 ± 1.37
FSM-5	800	0.70 ± 0.04	1.27 ± 0.06	0.36 ± 0.02	11.33 ± 0.75					-0.06 ± 0.01	1.73 ± 0.49
FSM-6	800			0.57 ± 0.29	6.08 ± 2.34	0.48 ± 0.24	27.76 ± 13.17			0.00 ± 0.03	1.17 ± 0.84
FSM-6LH	800	*Not measured due to very high signal intensities saturating the PMT despite adding an ND 2.0 filter.*									
CLBR	800	0.87 ± 0.12	3.99 ± 0.19			0.17 ± 0.07	32.27 ± 4.65			-0.03 ± 0.01	3.34 ± 1.54

*Table S1b: Lifetimes for the **blue IRSL$_{50}$** emission recorded in the **off-time** of the pulsed IRSL signal. I_i is the normalised intensity of the fitted lifetime τ_i (µs), k is a constant linear background. All values displayed are the average of three aliquots and the standard deviation. The data was normalised to the last data point of the on-time.*

Sample ID	Dose (Gy)	I_1	τ_1	I_2	τ_2	I_3	τ_3	I_4	τ_4	k	residual sum of squares
FSM-13	50			0.43 ± 0.13	5.25 ± 0.59	0.47 ± 0.14	13.27 ± 2.58	0.12 ± 0.02	39.99 ± 6.65	0.01 ± 0.00	0.88 ± 0.28
FSM-13LH	50							0.96 ± 0.02	45.08 ± 0.27	0.06 ± 0.00	0.63 ± 0.13
FSM-3	50	0.53 ± 0.08	0.73 ± 0.09	0.31 ± 0.05	6.65 ± 0.28			0.18 ± 0.04	23.08 ± 1.29	0.01 ± 0.00	0.11 ± 0.05
FSM-5	50	0.89 ± 0.04	0.83 ± 0.03	0.14 ± 0.02	7.52 ± 1.03			0.08 ± 0.01	24.39 ± 5.40	0.00 ± 0.00	0.16 ± 0.04
FSM-6	50			0.57 ± 0.10	6.64 ± 0.99			0.33 ± 0.05	24.24 ± 3.49	0.01 ± 0.00	0.58 ± 0.49
FSM-6LH	50							0.96 ± 0.01	43.08 ± 0.76	0.05 ± 0.00	0.21 ± 0.03
CLBR	50			0.78 ± 0.05	3.74 ± 0.26	0.16 ± 0.03	14.65 ± 2.13	0.03 ± 0.03	102.18 ± 64.17	0.06 ± 0.00	0.17 ± 0.08
FSM-13	200			0.40 ± 0.18	4.58 ± 1.63	0.45 ± 0.13	12.94 ± 3.26	0.11 ± 0.06	40.38 ± 8.46	0.001 ± 0.00	1.33 ± 0.45
FSM-13LH	200							0.99 ± 0.03	44.40 ±0.38	0.06 ± 0.00	1.12 ± 0.39
FSM-3	200	0.51 ± 0.10	0.67 ± 0.13	0.32 ± 0.05	5.84 ± 0.61			0.20 ± 0.03	22.16 ± 0.86	0.01 ± 0.00	0.27 ± 0.09
FSM-5	200	0.71 ± 0.05	0.81 ± 0.08	0.21 ± 0.02	6.92 ± 1.05			0.10 ± 0.02	23.33 ± 2.93	0.00 ± 0.00	0.38 ± 0.12
FSM-6	200			0.63 ± 0.11	6.50 ± 1.07			0.38 ± 0.08	25.90 ± 5.09	0.02 ± 0.01	1.66 ± 1.48
FSM-6LH	200							0.96 ± 0.00	41.71 ± 0.18	0.05 ± 0.00	0.64 ± 0.65
CLBR	200			0.82 ± 0.04	3.58 ± 0.06	0.18 ± 0.01	15.55 ± 1.79	0.03 ± 0.02	87.11 ± 31.14	0.03 ± 0.00	0.40 ± 0.24
FSM-13	800			0.51 ± 0.18	5.38 ± 1.20	0.47 ± 0.11	14.92 ± 2.69	0.06 ± 0.04	53.26 ± 15.37	0.01 ± 0.00	2.46 ± 1.32
FSM-13LH	800	*Not measured due to very high signal intensities saturating the PMT despite adding an ND 2.0 filter.*									
FSM-3	800	0.45 ± 0.04	0.74 ± 0.26	0.36 ± 0.09	6.31 ± 1.64			0.21 ± 0.03	23.01 ± 3.36	0.01 ± 0.00	0.76 ± 0.36
FSM-5	800	0.64 ± 0.06	0.86 ± 0.03	0.29 ± 0.02	6.96 ± 0.34			0.12 ± 0.01	24.06 ± 2.65	0.01 ± 0.00	0.27 ± 0.06
FSM-6	800			0.59 ± 0.15	6.78 ± 1.32			0.37 ± 0.10	24.78 ± 4.03	0.01 ± 0.01	0.55 ± 0.47
FSM-6LH	800	*Not measured due to very high signal intensities saturating the PMT despite adding an ND 2.0 filter.*									
CLBR	800			0.76 ± 0.09	3.49 ± 0.18	0.18 ± 0.02	13.91 ± 1.38	0.04 ± 0.04	68.07 ± 37.48	0.03 ± 0.00	1.15 ± 0.73

*Table S2a: Lifetimes for the **blue post-IR IRSLI$_{225}$** emission recorded in the **on-time** of the pulsed IRSL signal. I_i is the normalised intensity of the fitted lifetime τ_i (μs), k is a constant linear background. All values displayed are the average of three aliquots and the standard deviation. The data was normalised to the last data point of the on-time.*

Sample ID	Dose (Gy)	I_1	τ_1	I_2	τ_2	I_3	τ_3	I_4	τ_4	k	residual sum of squares
FSM-13	50	0.53 ± 0.04	4.66 ± 0.07	0.48 ± 0.07	21.25 ± 3.95					0.03 ± 0.02	2.08 ± 0.87
FSM-13LH	50					1.28 ± 0.02	57.05 ± 1.16			0.26 ± 0.01	0.10 ± 0.02
FSM-3	50	0.71 ± 0.07	1.25 ± 0.10	0.19 ± 0.01	16.00 ± 1.58					0.13 ± 0.07	0.96 ± 0.42
FSM-5	50	0.80 ± 0.06	1.18 ± 0.02	0.29 ± 0.04	10.92 ± 3.50					-0.09 ± 0.01	1.01 ± 0.56
FSM-6	50			0.95 ± 0.04	10.94 ± 1.56					0.05 ± 0.03	0.70 ± 0.37
FSM-6LH	50					1.16 ± 0.04	32.53 ± 2.63			0.09 ± 0.01	0.04 ± 0.02
CLBR	50	0.81 ± 0.20	4.40 ± 0.37			0.31 ± 0.26	34.18 ± 17.84			0.04 ± 0.06	0.44 ± 0.23
FSM-13	200	0.60 ± 0.03	4.93 ± 0.67			0.39 ± 0.07	24.92 ± 5.48			0.01 ± 0.01	4.34 ± 0.14
FSM-13LH	200					1.24 ± 0.05	52.93 ± 1.67			0.25 ± 0.00	0.17 ± 0.04
FSM-3	200	0.63 ± 0.05	1.20 ± 0.08	0.17 ± 0.01	14.48 ± 0.06					0.17 ± 0.08	2.25 ± 0.82
FSM-5	200	0.80 ± 0.04	1.21 ± 0.08	0.25 ± 0.01	8.16 ± 1.29					-0.07 ± 0.01	2.34 ± 0.73
FSM-6	200			0.93 ± 0.07	10.61 ± 1.28					0.04 ± 0.03	1.23 ± 0.70
FSM-6LH	200					1.21 ± 0.03	35.87 ± 1.39			0.09 ± 0.00	0.28 ± 0.22
CLBR	200	0.80 ± 0.16	4.14 ± 0.24			0.24 ± 0.25[b]	29.73 ± 6.83[b]			0.06 ± 0.01	1.64 ± 0.72
FSM-13	800	0.57 ± 0.06	4.63 ± 0.41	0.45 ± 0.03	16.77 ± 2.37					0.00 ± 0.01	7.14 ± 3.32
FSM-13LH	800	*Not measured due to very high signal intensities saturating the PMT despite adding an ND 2.0 filter.*									
FSM-3	800	0.56 ± 0.14	1.26 ± 0.22	0.16 ± 0.01	14.39 ± 1.78					0.26 ± 0.12	6.52 ± 2.69
FSM-5	800	0.77 ± 0.02	1.23 ± 0.04	0.32 ± 0.02	8.25 ± 1.38					-0.06 ± 0.01	1.59 ± 0.48
FSM-6	800			0.97 ± 0.02	10.06 ± 0.88					0.03 ± 0.02	0.44 ± 0.29
FSM-6LH	800	*Not measured due to very high signal intensities saturating the PMT despite adding an ND 2.0 filter.*									
CLBR	800	0.79 ± 0.21	3.95 ± 0.38			0.45[a]	25.64[a]			0.06 ± 0.00	5.26 ± 2.42

*Table S2b: Lifetimes for the **blue post-IR IRSL$_{225}$** emission recorded in the **off-time** of the pulsed IRSL signal. I_i is the normalised intensity of the fitted lifetime τ_i (μs), k is a constant linear background. All values displayed are the average of three aliquots and the standard deviation. The data was normalised to the last data point of the on-time.*

Sample ID	Dose (Gy)	I_1	τ_1	I_2	τ_2	I_3	τ_3	I_4	τ_4	k	residual sum of squares
FSM-13	50			0.45 ± 0.07	4.13 ± 0.27	0.35 ± 0.05	14.31 ± 2.46	0.12 ± 0.02	39.99 ± 6.65	0.01 ± 0.00	0.88 ± 0.28
FSM-13LH	50							0.96 ± 0.02	45.08 ± 0.27	0.06 ± 0.00	0.63 ± 0.13
FSM-3	50	0.65 ± 0.07	0.89 ± 0.07	0.14 ± 0.02	7.52 ± 0.89			0.18 ± 0.04	23.08 ± 1.29	0.01 ± 0.00	0.11 ± 0.05
FSM-5	50	0.75 ± 0.05	0.90 ± 0.03	0.27 ± 0.03	8.82 ± 2.09			0.08 ± 0.01	24.39 ± 5.40	0.00 ± 0.00	0.16 ± 0.04
FSM-6	50			0.77 ± 0.12	8.95 ± 0.27			0.33 ± 0.05	24.24 ± 3.49	0.01 ± 0.00	0.58 ± 0.49
FSM-6LH	50							0.96 ± 0.01	43.08 ± 0.76	0.05 ± 0.00	0.12 ± 0.03
CLBR	50			0.73 ± 0.20	3.96 ± 0.32	0.12 ± 0.06	20.81 ± 7.25	0.03 ± 0.03	102.18 ± 64.17	0.06 ± 0.05	0.31 ± 0.29
FSM-13	200			0.45 ± 0.13	3.81 ± 0.80	0.37 ± 0.09	14.33 ± 4.51	0.11 ± 0.07	62.84 ± 39.90	0.05 ± 0.01	1.96 ± 0.73
FSM-13LH	200							0.77 ± 0.02	44.37 ± 0.04	0.27 ± 0.00	0.46 ± 0.12
FSM-3	200	0.57 ± 0.06	0.84 ± 0.11	0.13 ± 0.01	6.62 ± 1.48			0.08 ± 0.02	33.25 ± 1.37	0.22 ± 0.07	2.45 ± 1.24
FSM-5	200	0.73 ± 0.02	0.84 ± 0.03	0.28 ± 0.02	5.90 ± 0.76			0.03 ± 0.01	33.28 ± 2.88	0.01 ± 0.00	0.31 ± 0.09
FSM-6	200			0.77 ± 0.13	8.81 ± 0.19			0.16 ± 0.07	32.15 ± 4.08	0.07 ± 0.01	0.89 ± 0.67
FSM-6LH	200							0.90 ± 0.00	37.86 ± 0.31	0.10 ± 0.00	0.47 ± 0.37
CLBR	200			0.72 ± 0.15	3.71 ± 0.11	0.11 ± 0.04	14.05 ± 1.67	0.08 ± 0.12	94.63 ± 42.70	0.12 ± 0.02	1.25 ± 0.70
FSM-13	800			0.38 ± 0.10	3.41 ± 0.42	0.48 ± 0.06	10.96 ± 3.37	0.13 ± 0.08	37.63 ± 14.26	0.05 ± 0.00	3.51 ± 1.50
FSM-13LH	800	*Not measured due to very high signal intensities saturating the PMT despite adding an ND 2.0 filter.*									
FSM-3	800	0.52 ± 0.11	0.84 ± 0.20	0.15 ± 0.04	7.80 ± 1.80			0.06 ± 0.02	37.87 ± 4.60	0.29 ± 0.11	7.88 ± 3.03
FSM-5	800	0.69 ± 0.01	0.87 ± 0.04	0.32 ± 0.02	6.01 ± 0.58			0.05 ± 0.01	32.31 ± 3.06	0.02 ± 0.00	0.29 ± 0.07
FSM-6	800			0.85 ± 0.06	9.10 ± 0.17			0.11 ± 0.05	34.26 ± 3.42	0.07 ± 0.01	0.29 ± 0.24
FSM-6LH	800	*Not measured due to very high signal intensities saturating the PMT despite adding an ND 2.0 filter.*									
CLBR	800			0.70 ± 0.15	3.52 ± 0.32	0.10 ± 0.04	11.18 ± 1.97	0.10 ± 0.14	133.61 ± 111.59	0.12 ± 0.00	4.33 ± 3.14

*Table S3a: Lifetimes for the **yellow-green IRSL$_{50}$** emission recorded in the **on-time** of the pulsed IRSL signal. I_i is the normalised intensity of the fitted lifetime τ_i (ms), k is a constant linear background. All values displayed are the average of three aliquots and the standard deviation. The data was normalised to the last data point of the on-time.*

Sample ID	Dose (Gy)	I_1	τ_1	I_2	τ_2	I_3	τ_3	I_4	τ_4	k	residual sum of squares
FSM-13	200	0.20 ± 0.01	0.22 ± 0.08	0.83 ± 0.02	2.50 ± 0.34					0.09 ± 0.01	0.06 ± 0.03
FSM-13LH	200	0.64 ± 0.06	0.05 ± 0.00	0.12 ± 0.05	2.52 ± 0.43					0.26 ± 0.00	0.01 ± 0.01
FSM-3	200	0.09 ± 0.03	0.02 ± 0.01			1.87 ± 0.18	8.52 ± 0.61			0.18 ± 0.02	0.04 ± 0.01
FSM-5	400	0.39 ± 0.01	0.02 ± 0.00	0.14 ± 0.00	3.93 ± 0.72					0.51 ± 0.01	0.27 ± 0.14
FSM-6	400	0.43 ± 0.14	0.04 ± 0.00	0.38 ± 0.49	4.04 ± 1.46					0.36 ± 0.11	0.05 ± 0.04
FSM-6LH	200	0.66 ± 0.01	0.04 ± 0.00	0.07 ± 0.00	2.13 ± 0.28					0.28 ± 0.00	0.01 ± 0.00
CLBR	200	0.10[a]	0.03[a]			2.43 ± 0.21	11.12 ± 1.55			0.13 ± 0.01	0.05 ± 0.05
FSM-13	800	0.20 ± 0.00	0.20 ± 0.04	0.82 ± 0.03	2.37 ± 0.19					0.09 ± 0.01	0.01 ± 0.01
FSM-13LH	800	0.66 ± 0.02	0.05 ± 0.00	0.08 ± 0.00	1.81 ± 0.08					0.27 ± 0.00	0.02 ± 0.01
FSM-3	800	0.11 ± 0.02	0.03 ± 0.01			1.57 ± 0.20	8.10 ± 0.67			0.20 ± 0.03	0.02 ± 0.01
FSM-5	800	0.38 ± 0.04	0.04 ± 0.00	0.15 ± 0.06	4.10 ± 2.38					0.53 ± 0.01	0.19 ± 0.06
FSM-6	800	0.37 ± 0.12	0.04 ± 0.00	0.65 ± 0.47	6.16 ± 1.76					0.31 ± 0.09	0.09 ± 0.06
FSM-6LH	800	0.64 ± 0.01	0.05 ± 0.00	0.08 ± 0.00	1.82 ± 0.41					0.27 ± 0.00	0.02 ± 0.01
CLBR	800	0.06[a]	0.04[a]			2.22 ± 0.10	9.66 ± 0.17			0.12 ± 0.01	0.01 ± 0.01

*Table S3b: Lifetimes for the **yellow-green IRSL$_{50}$** emission recorded in the **off-time** of the pulsed IRSL signal. I_i is the normalised intensity of the fitted lifetime τ_i (ms), k is a constant linear background. All values displayed are the average of three aliquots and the standard deviation. The data was normalised to the last data point of the on-time.*

Sample ID	Dose (Gy)	I_1	τ_1	I_2	τ_2	I_3	τ_3	I_4	τ_4	k	residual sum of squares
FSM-13	200	0.19 ± 0.03	0.24 ± 0.06	0.57 ± 0.02	2.19 ± 0.17	0.14 ± 0.04	9.58 ± 1.12			0.01 ± 0.00	0.05 ± 0.02
FSM-13LH	200	0.52 ± 0.02	0.12 ± 0.01	0.07 ± 0.04	6.09 ± 0.39					0.03 ± 0.02	0.15 ± 0.04
FSM-3	200	0.13 ± 0.01	0.11 ± 0.01			0.75 ± 0.04	11.04 ± 0.06			0.03 ± 0.01	0.14 ± 0.08
FSM-5	400	0.40 ± 0.01	0.09 ± 0.00			0.08 ± 0.00	10.18 ± 0.70			0.06 ± 0.00	0.39 ± 0.04
FSM-6	400	0.37 ± 0.13	0.10 ± 0.00	0.08 ± 0.06	5.35 ± 2.24	0.15 ± 0.23	32.98 ± 21.06			0.03 ± 0.02	0.19 ± 0.00
FSM-6LH	200	0.52 ± 0.00	0.11 ± 0.00	0.04 ± 0.00	6.55 ± 0.06					0.01 ± 0.00	0.17 ± 0.18
CLBR	200			0.17 ± 0.05	3.90 ± 1.34	0.75 ± 0.03	13.53 ± 0.90			0.08 ± 0.01	0.21 ± XX
FSM-13	800	0.20 ± 0.01	0.24 ± 0.03	0.58 ± 0.01	2.13 ± 0.09	0.13 ± 0.02	8.56 ± 0.96			0.01 ± 0.00	0.02 ± 0.01
FSM-13LH	800	0.53 ± 0.01	0.11 ± 0.00	0.04 ± 0.00	6.52 ± 0.06					0.02 ± 0.00	0.18 ± 0.02
FSM-3	800	0.24 ± 0.16	0.10 ± 0.01			0.51 ± 0.37	10.55 ± 0.51			0.04 ± 0.00	0.15 ± 0.12
FSM-5	800	0.31 ± 0.16	0.10 ± 0.02			0.23 ± 0.25	9.59 ± 0.12			0.11 ± 0.11	0.23 ± 0.05
FSM-6	800	0.32 ± 0.12	0.10 ± 0.01	0.11 ± 0.04	4.23 ± 2.34	0.23 ± 0.18	19.80 ± 11.31			0.02 ± 0.02	0.21 ± 0.04
FSM-6LH	800	0.52 ± 0.01	0.11 ± 0.00	0.05 ± 0.00	6.33 ± 0.15					0.01 ± 0.00	0.17 ± 0.01
CLBR	800	0.04[a]	0.14[a]	0.24 ± 0.02	5.34 ± 0.29	0.69 ± 0.04	14.90 ± 0.31			0.07 ± 0.02	0.06 ± 0.05

*Table S4a: Lifetimes for the **yellow-green post-IR IRSL$_{225}$** emission recorded in the **on-time** of the pulsed IRSL signal. I_i is the normalised intensity of the fitted lifetime τ_i (ms), k is a constant linear background. All values displayed are the average of three aliquots and the standard deviation. The data was normalised to the last data point of the on-time. [a]Only one aliquot of the three aliquots measured revealed this lifetime.*

Sample ID	Dose (Gy)	I_1	τ_1	I_2	τ_2	I_3	τ_3	I_4	τ_4	k	residual sum of squares
FSM-13	200	0.32 ± 0.03	0.12 ± 0.04	0.52 ± 0.04	1.92 ± 0.41					0.21 ± 0.02	0.07 ± 0.04
FSM-13LH	200	0.57 ± 0.00	0.05 ± 0.00	0.19 ± 0.00	2.06 ± 0.03					0.26 ± 0.00	0.01 ± 0.00
FSM-3	200	0.08 ± 0.01	0.03 ± 0.01			1.18 ± 0.20	7.14 ± 0.81			0.33 ± 0.03	0.11 ± 0.03
FSM-5	400	0.37[a]	0.02[a]	0.11[a]	2.80[a]					0.54	0.22
FSM-6	400	0.38 ± 0.02	0.04 ± 0.01	0.16 ± 0.01	2.35 ± 0.52					0.49 ± 0.00	0.06 ± 0.03
FSM-6LH	200	0.59 ± 0.00	0.04 ± 0.00	0.09 ± 0.01	1.59 ± 0.15					0.32 ± 0.00	0.01 ± 0.00
CLBR	200	0.24[a]	0.04[a]			2.39 ± 0.72	15.48 ± 4.07			0.31 ± 0.08	0.06 ± 0.06
FSM-13	800	0.32 ± 0.02	0.11 ± 0.01	0.52 ± 0.03	1.73 ± 0.18					0.19 ± 0.01	0.02 ± 0.01
FSM-13LH	800	0.56 ± 0.00	0.05 ± 0.00	0.19 ± 0.01	2.07 ± 0.12					0.27 ± 0.00	0.01 ± 0.00
FSM-3	800	0.08 ± 0.02	0.07 ± 0.07			1.10 ± 0.08	6.96 ± 0.56			0.35 ± 0.04	0.06 ± 0.02
FSM-5	800	0.33 ± 0.10	0.05 ± 0.03	0.09 ± 0.04	1.99 ± 0.63					0.58 ± 0.07	0.28 ± 0.11
FSM-6	800	0.44 ± 0.05	0.03 ± 0.00	0.13 ± 0.06	1.91 ± 0.30					0.46 ± 0.03	0.05 ± 0.04
FSM-6LH	800	0.59 ± 0.02	0.04 ± 0.00	0.11 ± 0.01	1.41 ± 0.36					0.31 ± 0.00	0.02 ± 0.01
CLBR	800	0.19[a]	0.05[a]			2.07 ± 0.45	12.35 ± 2.25			0.27 ± 0.06	0.02 ± 0.02

*Table S4b: Lifetimes for the **yellow-green post-IR IRSL$_{225}$** emission recorded in the **off-time** of the pulsed IRSL signal. I_i is the normalised intensity of the fitted lifetime τ_i (ms), k is a constant linear background. All values displayed are the average of three aliquots and the standard deviation. The data was normalised to the last data point of the on-time. [a]Only one aliquot of the three aliquots measured revealed this lifetime.*

Sample ID	Dose (Gy)	I_1	τ_1	I_2	τ_2	I_3	τ_3	I_4	τ_4	k	residual sum of squares
FSM-13	200	0.33 ± 0.05	0.18 ± 0.04	0.33 ± 0.04	1.58 ± 0.02	0.12 ± 0.05	10.13 ± 0.82			0.07 ± 0.01	0.09 ± 0.03
FSM-13LH	200	0.47 ± 0.00	0.12 ± 0.00	0.10 ± 0.00	2.81 ± 0.09	0.05 ± 0.00	16.35 ± 0.79			0.05 ± 0.00	0.11 ± 0.00
FSM-3	200	0.13 ± 0.01	0.12 ± 0.02			0.56 ± 0.04	9.54 ± 0.22			0.18 ± 0.03	0.44 ± 0.12
FSM-5	400	0.42 ± 0.02	0.09 ± 0.00			0.05 ± 0.00	9.64 ± 0.70			0.02 ± 0.00	0.31 ± 0.07
FSM-6	400	0.40 ± 0.02	0.09 ± 0.00	0.06 ± 0.01	2.46 ± 0.31	0.06 ± 0.01	12.67 ± 0.03			0.06 ± 0.01	0.16 ± 0.02
FSM-6LH	200	0.50 ± 0.00	0.11 ± 0.00	0.04 ± 0.00	3.57 ± 0.07	0.01 ± 0.00	28.54 ± 2.43			0.02 ± 0.00	0.16 ± 0.01
CLBR	200	0.22[a]	0.14[a]			0.57 ± 0.03	11.36 ± 0.18	0.21 ± 0.00[b]	56.08 ± 17.86[b]	0.19 ± 0.08	0.23 ± 0.11
FSM-13	800	0.32 ± 0.02	0.18 ± 0.01	0.36 ± 0.03	1.58 ± 0.13	0.10 ± 0.03	9.87 ± 1.10			0.07 ± 0.01	0.04 ± 0.01
FSM-13LH	800	0.46 ± 0.00	0.12 ± 0.00	0.10 ± 0.00	2.68 ± 0.04	0.05 ± 0.00	16.15 ± 0.32			0.05 ± 0.00	0.11 ± 0.00
FSM-3	800	0.14 ± 0.02	0.12 ± 0.01			0.60 ± 0.09	9.73 ± 0.99			0.14 ± 0.10	0.22 ± 0.13
FSM-5	800	0.40 ± 0.02	0.09 ± 0.00			0.07 ± 0.01	7.23 ± 0.30			0.02 ± 0.00	0.25 ± 0.03
FSM-6	800	0.41 ± 0.03	0.09 ± 0.00	0.05 ± 0.02	4.13 ± 3.30	0.05 ± 0.01	13.96 ± 1.24			0.06 ± 0.01	0.18 ± 0.02
FSM-6LH	800	0.50 ± 0.00	0.11 ± 0.00	0.05 ± 0.00	3.30 ± 0.16	0.02 ± 0.00	21.06 ± 2.90			0.03 ± 0.00	0.16 ± 0.00
CLBR	800	0.17[a]	0.12[a]			0.36 ± 0.20	8.30 ± 3.36	0.37 ± 0.11	22.71 ± 7.49	0.19 ± 0.08	0.10 ± 0.07

1